Published in final edited form as:
Adv Drug Deliv Rev. 2014 June 15; 0: 94–109. doi:10.1016/j.addr.2014.01.008.

Ultrasound-mediated blood-brain barrier disruption for targeted drug delivery in the central nervous system

Muna Aryal, B.S.[a,b], **Costas D. Arvanitis, Ph.D.**[b], **Phillip M. Alexander, M.D.**[c], and **Nathan McDannold, Ph.D.**[b]

[a]Department of Physics, Boston College, Chestnut Hill, USA

[b]Department of Radiology, Brigham & Women's Hospital, Harvard Medical School, Boston, USA

[c]Department of Engineering Science, Brasenose College, University of Oxford, Oxford, UK

Abstract

The physiology of the vasculature in the central nervous system (CNS), which includes the blood-brain barrier (BBB) and other factors, complicates the delivery of most drugs to the brain. Different methods have been used to bypass the BBB, but they have limitations such as being invasive, non-targeted or requiring the formulation of new drugs. Focused ultrasound (FUS), when combined with circulating microbubbles, is a noninvasive method to locally and transiently disrupt the BBB at discrete targets. This review provides insight on the current status of this unique drug delivery technique, experience in preclinical models, and potential for clinical translation. If translated to humans, this method would offer a flexible means to target therapeutics to desired points or volumes in the brain, and enable the whole arsenal of drugs in the CNS that are currently prevented by the BBB.

Keywords

Brain; Drug Delivery; Ultrasound; Microbubbles

1. Introduction

The blood-brain barrier (BBB) is a specialized non-permeable barrier in cerebral microvessels consisting of endothelial cells connected together by tight junctions, a thick basement membrane, and astrocytic endfeet. The tight junctions between the endothelial cells, together with an ensemble of enzymes, receptors, transporters, and efflux pumps of the multidrug resistance (MDR) pathways, control and limit access of molecules in the vascular compartment to the brain by paracellular or transcellular pathways [1]. The BBB normally

Corresponding Author: Nathan McDannold 75 Francis Street Boston, MA 02115 P: 617 278-0605; F: 617 525-7450 njm@bwh.harvard.edu.

protects the brain from toxins, and helps maintain the delicate homeostasis of the neuronal microenvironment. However, it also excludes 98% of small-molecule drugs and approximately 100% of large-molecule neurotherapeutics from the brain parenchyma [2,3]. Only small-molecule drugs with high lipid solubility and a molecular mass under 400–500 Da can cross the BBB in pharmacologically significant amounts, resulting in effective treatments for only a few diseases such as depression, affective disorders, chronic pain, and epilepsy. Given the paucity of small-molecule drugs effective for CNS disorders, it is clear that the BBB is a primary limitation for the development and use of drugs in the brain. Overcoming this hindrance could mean potential therapies for a wide range of disorders, including Alzheimer's and Huntington's diseases, amyotrophic lateral sclerosis (ALS), neuro-AIDS, stroke, brain or spinal cord trauma, autism, lysosomal storage disorders, fragile X syndrome, inherited ataxias, and blindness.

Tumors, particularly those in the brain also face challenges for effective drug delivery. While the blood vessels in most primary and metastatic brain tumors are often somewhat permeable from the lack of a fully formed BBB, infiltrating cancer cells at the tumor margins and small metastatic seeds may be protected by the BBB of surrounding normal tissue [4]. Glioblastomas in particular are highly infiltrative, and commonly recur after localized treatments such as conformal radiotherapy or surgery. Relapse usually occurs within a few centimeters of the treatment site [5–7]. Furthermore, their vascular permeability is heterogeneous, and additional barriers to drug delivery include increased interstitial pressures [8] and drug efflux pumps that contribute to their multidrug resistance phenotype [9]. As for metastatic tumors, work in mice suggests that the blood-tumor barrier (BTB) is only partially compromised in breast adenocarcinoma brain metastases, and that toxic concentrations of chemotherapy are only achieved in a small subset of tumors that are highly permeable [10]. Also, systemic drug accumulation in brain metastases can be substantially less than in extracranial metastases [10]. Thus, the BTB is a hindrance to effective drug delivery similarly to the BBB.

2. Methods for Drug Delivery in the Brain

In order to overcome these limitations, it is necessary to either bypass these vascular barriers altogether, or to facilitate passage across it via controlled exploitation of endogenous transport mechanisms. Different methods have been explored to bypass the BBB (or the BTB) (Table 1) [11–13]. While these methods are promising, they also have limitations.

2.1 Invasive Approaches to Brain Drug Delivery

High local drug concentrations can be achieved by inserting a needle or catheter into the brain and directly injecting or infusing drugs or by implanting drug-exuding devices. With such techniques, therapeutic benefits have been shown for brain tumors and other disorders [14–17]. However, because of their invasiveness, there are some risks of infection or brain trauma, and they may not be amenable for repeated treatments or for drug delivery to large areas of the brain. It can also be a challenge to control the drug distribution, as drug concentrations decrease exponentially from the injection or implantation site [18]. When convection-enhanced diffusion is used, the infused agents are delivered preferentially along white matter tracts [19], which may not be desirable.

Another approach for bypassing the BBB is to introduce drugs into the cerebrospinal fluid (CSF) via intrathecal or intraventricular routes. It then follows the flow patterns of the CSF and enters the brain parenchyma via diffusion. This approach has been successful in cases where the target is in the subarachnoid space [20], but drug diffusion drops off exponentially from the brain surface and penetration into the brain parenchyma can be limited [11]. It is also possible to deliver drugs transnasally from the submucus space into the olfactory CSF [21–24]. This approach has advantages of being noninvasive and being relatively easy to administer. However, only small drug volumes can be delivered and interindividual variability and other factors may pose challenges to this procedure [24]. Nevertheless, the technique is a promising route to bypass the BBB and is currently being investigated by numerous researchers.

2.2 Transvascular Brain Drug Therapy: Biopharmaceutical Approaches

A number of approaches have been investigated to develop or modify drugs that can cross the BBB. While these methods are highly promising and offer the ability to easily administer drugs to the CNS as in other organs, they do require the expense and time of developing new agents, and they result in drugs being delivered to the entire brain, which may not always be desirable.

Converting water-soluble molecules that would not ordinarily cross the BBB into lipid-soluble ones is one approach to brain drug therapy. This can be achieved by the addition of lipid groups, or functional groups such as acetate to block hydrogen bonding. The molecule would then undergo passive diffusion across the BBB. An example of this is the conversion of morphine to heroine by the acetylation of two hydroxyl groups, which results in the removal of the molecule from hydrogen bonding with its aqueous environment [25]. Although utilized by the pharmaceutical industry, this approach has limited applicability to drugs greater than 400–450 Da [12,26].

Another approach involves utilizing the large variety of solute carrier proteins (SLC) on the endothelial surface that specifically transport many essential polar and charged nutrients such as glucose, amino acids, vitamins, small peptides, and hormones transcellularly across the BBB [27]. These transporters move the solute into the cytoplasm where they await another SLC at the opposite cell membrane to exocytose them into the brain parenchyma. An example of SLC used for brain drug therapy is the large neutral amino acid transporter type 1 (LAT1), which transports the amino acid Parkinson's drug L-dopa across the BBB. Once across, it is converted to dopamine by aromatic amino acid decarboxylase, and can then bind to its target receptor. Dopamine being water-soluble cannot cross the BBB [26,28].

Finally, the molecular targeting of endothelial-surface receptors, colloquially termed the “Trojan Horse” approach, is yet another paradigm in drug transport across the BBB. This involves using a targeting ligand such as a serum protein, monoclonal antibody, or other high affinity targeting molecule that binds to its receptor and activates endocytosis of the complex into a vesicle that is transported across to, and released from the opposite pole (i.e., transcytosis). In theory, if the ligand is chemically linked to a drug or drug carrier, it too is transported across the BBB. Over the last two decades, a number of animal studies have

suggested the transport of antineoplastic drugs, fusion proteins, genetic therapies (plasmid vectors, siRNA), liposomes, and nanoparticles by this mechanism [29–32]. For transcytosis to occur, it requires that the endosome not fuse with lysosomes while in the cytoplasm, which would degrade the internalized macromolecules. Unlike other tissues, endothelial cells in brain capillaries appear to have low levels of endosome fusion with lysosomes, facilitating transport of necessary substances through the transcellular route [33–35].

2.3 Transvascular Brain Drug Therapy: BBB Disruption

Others have investigated methods to temporarily disrupt the BBB to enable CNS delivery of circulating agents. One such technique investigated intensively for several decades is the intraarterial injection of hyperosmotic solutions such as mannitol. This procedure causes shrinkage of endothelial cells and consequent stretching of tight junctions [36–39] through which drugs may pass. This method has been shown repeatedly to enhance delivery of therapeutic agents to brain tumors, and several promising clinical trials have been performed [40–45]. Other agents such as bradykinin have also been investigated [46–49]. While such methods can be an effective means to deliver drugs to large brain regions, they are invasive procedures that require general anesthesia, and can have side effects. For example, one study reported focal seizures in 5% of patients who received osmotic BBB disruption [40], and others have noted vasovagal response with bradycardia and hypotension [39]. Having a less-invasive way to achieve this disruption would be desirable.

The use of ultrasound, when combined with circulating microbubbles, offers a potential way to disrupt the BBB in a targeted, noninvasive, and repeatable manner to deliver a wide range of drugs to the brain and to brain tumors. Below, we review the literature on this technique, (i) describing how it is performed, (ii) how different parameters effect the BBB disruption, (iii) what has been delivered in preclinical studies, and (iv) methods that can be used to guide the procedure. While to date the technique has only been performed in animals, it is clear that it holds great promise for the treatment of a wide range of CNS disorders. If successfully translated to the clinic, it offers a means to target drugs, biomolecular therapies, and perhaps cellular therapies to desired brain regions while sparing the rest of the brain from unnecessary uptake. The technique also offers the potential to control the “magnitude” of BBB disruption at each focal target through modification of the ultrasound parameters, enabling a level of control over drug delivery that is not available with other technologies. This flexibility, along with its noninvasiveness, lack of need for general anesthesia, and amenability to be readily repeated make FUS a potentially transformative technology.

3. Focused Ultrasound

An ultrasound field can be noninvasively focused deep into the body and used to induce a broad range of bioeffects through thermal or mechanical mechanisms. FUS has been investigated since the 1940's for noninvasive ablation in the brain, as a potential alternative to surgical resection and radiosurgery [50–53]. Until recently, clinical testing required a craniotomy to allow for ultrasound propagation into the brain [54,55] because of ultrasonic heating of the skull, and beam aberration caused by the skull's irregular shape and large acoustic impedance.

In the past decade, FUS thermal ablation systems have been developed that overcome these obstacles produced by the skull [56]. They reduce skull heating through active cooling of the scalp and a transducer design with a large aperture to distribute the ultrasound energy over a large skull region, and they correct for beam aberrations using a phased array transducer design. When combined with methods that use acoustic simulation based on CT scans of the skull bone to determine the phase and amplitude corrections for the phased array [57,58] and MR temperature imaging (MRTI) to monitor the heating [59], a completely noninvasive alternative to surgical resection in the brain becomes possible. These systems use very high intensities to enable thermal ablation through the human skull, and are currently in initial human trials [60–63].

The effects of FUS can be enhanced by combining the ultrasound exposures (“sonications”) with preformed microbubbles that are commercially available as ultrasound imaging contrast agents. They consist of semi-rigid lipid or albumin shells that encapsulate a gas (typically a perfluorocarbon), range in size from about 1–10 μm, and are constrained to the vasculature. The microbubbles concentrate the ultrasound effects to the microvasculature, greatly reducing the FUS exposure levels needed to produce bioeffects. Thus, with microbubbles one can apply FUS transcranially without significant skull heating.

When microbubbles interact with an ultrasound field, a range of biological effects have been observed [64]. Depending on their size, the bubbles can oscillate within the ultrasound field, and they can grow in size via rectified diffusion. They can interact with the vessel wall through oscillatory and radiation forces [65,66]. They also can exert indirect shear forces induced by micro-streaming in the fluid that surrounds them [67]. At higher acoustic pressures, they can collapse during the positive pressure cycle, a phenomenon known as inertial cavitation, producing shock waves and high-velocity jets [65], free radicals [68], and high local temperatures [69,70]. The microbubbles used in ultrasound contrast agents can presumably exhibit these behaviors, either with their shells intact or after being broken apart by the ultrasound beam and their gas contents released.

4. Ultrasound-Induced BBB Disruption

Since the early years of investigation into ultrasound bioeffects on the brain, several studies have noted localized BBB disruption, either accompanied with tissue necrosis or without evident tissue damage [52,71–76]. None of these early studies however, elucidated sonication parameters that could repeatedly and reliably produce BBB disruption without occasionally producing lesions or necrosis.

In 2000 our laboratory found that if short ultrasound bursts are preceded by an intravenous injection of microbubble contrast agent, the BBB can be consistently opened without the production of lesions or apparent neuronal damage [77]. The circulating microbubbles appear to concentrate the ultrasound effects to the blood vessel walls, causing BBB disruption through widening of tight junctions and activation of transcellular mechanisms, with little effect on the surrounding parenchyma [78]. Furthermore, the opening occurs at acoustic power levels orders of magnitude lower than was previously used, making this method substantially easier to apply through the intact skull. For BBB disruption, the

sonications have been typically applied as short (~1–20 ms) bursts applied at a low duty cycle (1–5%) for 0.5–1 min. With a few simple modifications to enable low-intensity bursts, existing clinical brain FUS systems can be used for BBB disruption [79]. Clinical translation may also be possible using simpler FUS systems [80].

Figure 1 shows examples of targeted BBB disruption in a macaque from our institution using a clinical transcranial MRI-guided FUS system (ExAblate, InSightec, Haifa, Israel) [79]. The device uses a hemispherical 1024-element phased array operating at 220 kHz, and is integrated with a 3T MRI scanner. The focal region can be electronically steered to different locations using this array without physically moving the transducer. Volumes can be targeted by systematically steering the focal point to different targets, enabling one to deliver drugs to desired brain regions. Figure 2 shows an example of such “volumetric” FUS-induced BBB disruption. BBB disruption was evaluated using two MRI contrast agents and with the vital dye trypan blue. Note the lack of contrast enhancement in white matter despite evident staining with the dye. This difference is presumably due to the lower vascular density in white matter compared to gray matter.

4.1 Effect of Ultrasound Parameters and Other Factors on BBB Disruption

A number of sonication parameters can be varied in ultrasonic BBB disruption. Each parameter variation may impact the threshold pressure amplitude needed to disrupt the BBB, the magnitude of its disruption, and the resultant drug quantity delivered to the brain parenchyma. As determined from a number of studies, parameter variations and their effects are listed in Table 2. These studies used an MRI contrast agent, fluorescent probe, or drug to evaluate the BBB disruption. Given the large parameter space, and different techniques and criteria used to evaluate the disruption (each with different sensitivities), it can be challenging to compare results from different laboratories. Such comparisons are additionally confounded by uncertain accuracies in estimates of acoustic pressure amplitude when sonicating through the skull [81]. However, general trends can be observed.

For a fixed set of parameters, as one increases the pressure amplitude, the magnitude of the BBB disruption increases, and at some level it appears to saturate [82–84]. Below some value, no disruption is detected, and at some higher pressure threshold, vascular damage is produced along with the disruption (see below). Such studies repeated while varying a different parameter have shown that the threshold for BBB disruption depends strongly on the ultrasound frequency [85] and burst length [86]. Most experiments have been done with commercially-available ultrasound contrast agents that consist of microbubbles with a wide range of diameters. Experiments with microbubbles with narrow size distributions suggest that the BBB disruption threshold can also be reduced by using larger microbubbles [87–89].

By fixing the pressure amplitude and varying each parameter, one can evaluate their effects on the magnitude of the disruption. The magnitude has been found to increase with the burst length up to a duration of approximately 10 ms, with further increases in burst length having little or no effect [77,81,86,90,90–92]. Several groups have shown that the disruption magnitude may be increased by using a larger dose of ultrasound contrast agent [83,93–95] (although other works have shown little or no effect [86,90]) or by using larger

microbubbles [87–89]. Pulse repetition frequency can also influence the magnitude of disruption up to a point [90,91], but other studies have seen no dependence [86]. Finally, the magnitude of the disruption can be increased by increasing the sonication duration [84] or by repeating the sonication after some delay [96,97], but excessive durations may result in tissue damage [84,97]. Factors such as using an infusion instead of a bolus injection of microbubbles [98] and choice of anesthesia protocol [99] may also influence the resulting disruption. Other factors such as the delay between the microbubble injection and the start of sonication, and whether the drug or tracer is administered before or after the sonication may also be expected to have an effect. Additive effects have been observed when FUS-induced BBB disruption is combined with agents that affect vascular permeability [100–102].

These trends observed in parametric studies are difficult to interpret with confidence since the exact mechanism by which microbubble-enhanced FUS induces BBB disruption is currently unknown (see below). They are perhaps consistent with the following notions. First, for BBB disruption to occur, the microbubbles oscillations may need to reach a certain minimal radius, which can be achieved by increasing the pressure amplitude or by using larger microbubbles, and assuming the bubbles grow during each burst via rectified diffusion, by decreasing the ultrasound frequency or increasing the burst length. Next, in addition to depending on the bubble size during its oscillation, the magnitude of the disruption depends on the number of sites on which the microbubbles interact with the vasculature. The number of these sites can be increased by increasing the microbubble dose, or by increasing the sonication duration and/or number of bursts. Data showing a strong dependence on burst length may also suggest that the threshold and magnitude of the disruption depend on the amount of time the microbubbles interact with the blood vessels during each burst. Pulse repetition frequency may have an influence if the microbubbles are being fragmented or destroyed – time may be needed to replenish them if that is the case [103]. Finally, it appears that the magnitude of the disruption can saturate at some level, and increasing the different parameters has no additional effect.

4.2 Optimal Parameters?

Overall, these studies have made it clear that BBB disruption is possible over a wide range of exposure parameters. Disruption has been demonstrated at frequencies between 28 kHz [104] and 8 MHz [92], burst lengths as low as a few ultrasound cycles [90,91,98] up to 100 ms [77], and over a range of pulse repetition frequencies, microbubble doses, and sonication times. It is not clear what the “optimal” parameters are, or what criteria to use to establish them. In our view, the primary consideration could be to find parameters that maximize the window in acoustic pressure amplitude where robust BBB disruption is possible without producing vascular damage. It will be challenging to precisely estimate the pressure amplitude in the human brain after transcranial sonication, and having the widest safety margin possible will be desirable for clinical translation. How close the FUS frequency is to the “resonant size” of the microbubbles may have an impact on the width of this safety window. Additional important criteria would be to optimize the frequency and transducer geometry to produce the desired focal spot size, to effectively focus through the skull with minimal distortion, and if a phased array transducer is used, to be able to steer the focal region throughout the brain. It may also be desirable to find parameters that enable BBB

disruption in the shortest possible sonication time so that multiple targets can be targeted in a reasonable amount of time, and to maintain a safe dose of microbubbles.

4.3 Potential Mechanisms

Even though FUS exposures combined with microbubbles have been investigated to disrupt the BBB in numerous studies, the exact mechanism to open BBB still remains unknown. It does appear that two known effects that can be induced by FUS, bulk heating and inertial cavitation, are not responsible. Initial studies on the method utilized MRI-based temperature imaging [77] during the sonications, and no measureable heating was observed. Studies that recorded the acoustic emissions during the sonications [105–107] have found that BBB disruption can be achieved without wideband acoustic emission, which is a signature for inertial cavitation [53]. It also may not be the same mechanism utilized for so-called “sonoporation”, where transient pores in cell membranes created by sonication with microbubbles enable drugs to enter [108]. Those pores are rapidly resolved, while FUS-induced BBB disruption lasts for several hours.

Fundamentally, we do not know if the FUS/microbubble interactions physically modify the vessel walls, or if they are triggering a physiological response that includes temporary BBB breakdown. As described below, electron microscopy studies have shown delivery of tracers through widened tight junctions [78,109], which could be consistent with a direct physical force pulling them apart, as well as active transport [78,110]. Other work has shown the sonications can induce vascular spasm [111,112]. While the role of this spasm is not clear, it does make clear that the sonications can trigger a physiological response.

In the absence of bulk heating and inertial cavitation, we are left with mechanical effects induced during the microbubble oscillations in the ultrasound field. A number of effects are produced with potential to induce the observed BBB disruption. Microbubbles tend to move in the direction of the wave propagation via acoustic radiation force [66], which will bring them in contact with vessel endothelium. During oscillation, the shell of the microbubble can break, the bubbles can be fragmented into smaller bubbles, and they can grow via rectified diffusion. Microstreaming due to microbubble oscillations can induce biologically-significant shear stresses on the neighboring endothelium, and the oscillations produce inward forces that in extreme cases can pull the vessel wall inward [113]. Clearly, the behavior of a microbubble in an acoustic field is complex, and it can be different in free fluid than when constrained within a capillary [114].

4.4 Bioeffects Induced by FUS and Microbubbles

The BBB disruption can occur almost immediately with sonication [112] and appears to decay exponentially over several hours thereafter [77,82,96,115]. The amount of agent delivered across the barrier appears to be much larger in grey matter than in white matter, presumably due to differences in vascular density [79]. Several studies have found that the barrier appears to be largely restored in approximately 4–6 hours [77,82,96,109,115,116]; other experiments have observed low-level disruption at 24 hours after sonication or longer [89]. The source of this discrepancy is not clear, but it could be simply that more sensitive detection methods such as high-field MRI combined with large doses of MRI contrast agent

are capable of detecting low-level disruption missed in other works. The duration of the opening to different tracers appears to be reduced for larger tracers [115].

This window in time where the barrier is open is thought to be good for the prospect of delivering even long-circulating drugs, but not so long as to produce concern of toxicity arising from chronic BBB breakdown. Indeed, the appearance of the brain after BBB disruption in light microscopy appears to be normal [117], even after repeated weekly sessions [79]. Example histology obtained after BBB disruption is shown in Figure 3 The only major feature that has been observed in many studies is the presence of tiny clusters of extravasated red blood cells (petechiae) [118,119]. It is thought that these petechiae are formed during inertial cavitation, and experiments where no wideband emissions (a signature for inertial cavitation) were observed, no such extravasations were observed [105]. Some have suggested that wideband emissions can be observed without producing such petechiae [106]. While the presence of these petechiae is undesirable, their impact on the brain may be minimal. Investigations looking for apoptosis or ischemia, which may be expected if serious vascular damage were occurring, failed to observe anything more than a few individual damaged neurons, and long-term effects have not found evidence of neuronal damage with such sonications [118,120]. At excessive exposure levels, more severe vascular damage, parenchymal damage, and neuronal loss can occur [77,121]

Transmission electron microscopy (TEM) investigations have demonstrated an increase of cytoplasmic vesicles in endothelium and pericytes (suggestive of transcytosis), formation of trans-endothelial fenestrae, widened tight junctions, and transport of serum components across the BBB [78]. The use of a 44 kDa tracer molecule helped elucidate arterioles as the major sight of trans-endothelial vesicle transport (followed by capillaries then venules), and showed extensive tracer deposition in the endothelial paracellular space, basement membrane, and surrounding brain parenchyma [110]. Finally, using immunogold labeling, the disappearance of tight junction (TJ) proteins occludin, claudin-5, and ZO-1 were shown, along with opened endothelial junctions and tracer leakage at 1–4 hours post-sonication [109]. The TJ proteins reappeared at 6 and 24 hours. Examples showing tracer penetration across the BBB through widened tight junctions and vesicular transport are shown in Figure 4. Other work has shown down-regulation of the same TJ proteins along with their mRNA, and recovery to normal levels at 12 hours post-sonication [122]. Reorganization of connexin gap junction proteins have also been reported [123]. An increase of endothelial vesicles in normal [124] and tumor microvessels [125] have also been observed on TEM with an up-regulation of caveolin proteins/mRNA, suggesting that caveolae-mediated transcytosis (CMT) as a contributing mechanism for permeability. These researchers also found increased phosphorylation of Src and caveolin-1/2, noting that Src-induced phosphorylation of caveolins is a trigger for CMT [126].

Intracellular signaling cascades in response to mechanical stimulation by FUS-induced BBB disruption is likely, but has only recently been addressed. Increased phosphorylation of Akt and its downstream molecule GSK3β has been shown in neurons flanking the BBB disruption at 24 hours, well after tight junction reassembly [127]. Akt phosphorylation has been implicated in neuroprotection after stroke [128], while activation of the p38 JNK MAP kinases promote neuronal apoptosis [129,130]. Alonso et al. showed increased protein

ubiquitination in neurons not glia post sonication, no increase in heat shock proteins, and limited neuronal apoptosis at 24 hours in areas staining positive for extravasated albumin [131]. Ca^{2+} signaling has also been suggested as being stimulated by FUS-induced BBB disruption. Specifically, temporary disruption of the endothelial plasma membrane (i.e., sonoporation) can induce immediate transient changes of intracellular Ca^{2+} concentration in cells with direct contact with microbubbles, and delayed fluctuations in nearby cells [132]. When factoring in fluid shear induced in an *in vitro* flow channel (intended to mimic cerebral vessels), the membrane disruption and Ca^{2+} transients were much lower [133].

Multiphoton microscopy (MPM) has provided useful insights into the bioeffects of FUS-induced BBB disruption. Initial work with this technique demonstrated arteriolar vasospasm in 14/16 mice lasting up to 5 minutes (Figure 5), and interrupted cerebral blood flow [111]. Although this could cause ischemic injury, it has been noted that mice have enhanced vasomotor excitability over other rodents, such as rats [134]. Indeed, a similar study in rats showed vasospasm in only 25% of the vessels examined [112]. Initial work has also noted two forms of vessel dye leakage, rapid focal microdisruptions (3–9 seconds) that were prevalent at vessel bifurcations, and slow disruptions that were observed as a gradual increase in extravascular signal intensity [111]. Subsequent work noted three rather than two leakage types: (1) fast, characterized by rapid increase to peak intensity and rapid decrease, (2) sustained, described as rapid increase to peak which persisted for up to an hour, and (3) slow, a gradual increase to peak intensity [112]. The authors noted that differing vessel calibers have preferences for different leakage types, and interestingly, that distinct peak negative pressures also show preference for leakage types. Continuing work suggested correlation between fast leakage, common with high pressure amplitudes, and detachment of astrocyte endfeet from the vessel walls [135].

4.5 Delivery of Imaging/Therapeutic Agents and Tests in Animal Disease Models

One advantage of this method for targeted drug delivery in the brain is that it appears to be “drug neutral” – that is, it appears that many agents with a wide range of properties can be successfully delivered across the BBB and/or the BTB. A large number of imaging tracers (Table 3) and therapeutic agents (Table 4) which normally do not cross the BBB have been delivered to the brain or to brain tumor models with FUS and microbubbles. The amount of substance delivered and the distance from the blood vessels that it penetrates appears to depend on its size. This is evident in the examples shown in Figure 2, where less delivery of an albumin-bound MRI contrast agent (MW: ~67 kDa) was evident compared to a standard agent (MW: 928 Da) in a macaque. This is even more clear in the example shown in Figure 6, where delivery of fluorescent Dextrans with different molecular weights was examined after sonication in the mouse hippocampus. For 3,000 Da Dextrans, a relatively uniform fluorescence was observed; for the larger 70 kDa tracer, it was more concentrated near the blood vessels, and a 2000 kDa was found not to penetrate at all [136]. This result points to a need for close examination of how the delivery of large agents occurs – it may not be enough to look for the presence of the agent, but to also investigate whether it is delivered far enough from the vasculature at a high enough concentration to reach the desired target at a therapeutic level. Low-resolution methods such as MRI may not be sufficient for this

purpose. It may be possible, for example, for agents to make it past the endothelial cells but get trapped at the basement membrane [137].

4.5.1 Delivery of Therapeutics—A large number of therapeutic agents have also been delivered to the brain and to brain tumor models (Table 4). Many of the studies so far have investigated the delivery of chemotherapy agents, such as BCNU [138], doxorubicin [96], methotrexate [139], cytarabine [140], and temozolomide [141]. Enhanced delivery of chemotherapy packaged in liposomes [83,142], targeted liposomes [143] and magnetic particles [144–146], which allow for MRI-based tracking and enhanced delivery via magnetic targeting, have also been demonstrated (Figure 7). Other works have shown Trastuzumab, an antibody-based agent used for HER2-positive breast cancer [147,148], and boronophenylalanine, which is used for boron neutron capture therapy, can be delivered to the brain and to brain tumor models [149,150]. FUS-induced BBB disruption has also been shown to improve the delivery of natural killer cells in a brain tumor model [151]. Finally, a number of experiments have loaded chemotherapy and other agents into the microbubbles used for the disruption [146,152–155], which offers the possibility of achieving even higher local payload at the targeted region.

Delivering agents for neurodegenerative diseases, such as Alzheimer's, Huntington's, and Parkinson's disease, have also been an active area of research by several groups. A number of therapies for neurodegenerative diseases such as neuroprotective agents [153,156], antibodies [157,158], plasmid DNA [154], and siRNA [135] have all been successfully delivered across the BBB using FUS and microbubbles. Other investigations have shown that circulating neural progenitor cells [159] or viral vectors for gene therapy [160–162] can be delivered to the sonicated regions after FUS-induced BBB disruption. An example of delivery of adeno-associated virus serotype 9 via FUS-induced BBB disruption to the different cell populations in the mouse brain is shown in Figure 8.

4.5.2 Disease Models—While delivery of these agents is promising, one also needs to demonstrate that the amount of drug delivered – and the drug penetration – is sufficient to produce a therapeutic response. In some cases it is also important to demonstrate that the drug reaches the desired target and is active after it is delivered [156]. Several studies have shown that FUS enhancement of the BTB can slow tumor growth and/or improve survival in orthotopic murine models of primary or metastatic brain tumors [138,141,142,144,145,148,163]. While in some cases the response has been modest, several of these studies have seen substantial improvements. Using multiple treatments may be necessary to achieve a pronounced improvement [142]. One factor that has not been investigated in depth so far is to confirm that drugs can successfully be delivered to infiltrating tumor cells, which are a major feature in glioma and other primary tumors, and to metastatic “seeds”. Both can be protected by the normal BBB. The orthotopic models investigated so far do generally not have large infiltrating zones, and the benefit observed in studies so far may have been primarily due to FUS-enhanced permeability of the BTB. It may be challenging to get therapeutic levels to distant regions that are protected by the BBB. Some agents may have neurotoxic effects on the normal brain that may limit this ability.

Beyond brain tumors, a study by Jordão et al. showed that delivery of antibodies targeted to amyloid plaques can reduce the plaque burden in Alzheimer's disease model mice [158]. While the decrease was modest, with multiple treatment sessions this may be an effective treatment strategy. In an intriguing follow-up study, the same group recently showed that FUS-induced BBB disruption *alone* can reduce the size of the plaques, perhaps through the delivery of endogenous antibodies [164]. We anticipate that these studies are only the beginning, and that FUS has a large potential for Alzheimer's disease and other neurodegenerative disorders. Issues regarding the feasibility and safety of disrupting the BBB in large brain regions (or the whole brain – perhaps repeatedly) may be need further investigation, however.

4.6 Methods to Plan, Monitor, and Evaluate FUS-induced BBB Disruption

As described above, FUS-induced BBB disruption utilizes the mechanical interactions between microbubbles oscillating in the ultrasound field and the vasculature. These interactions critically depend on the exposure parameters as well as the vascular density and perhaps other properties of the vascular bed. The latter, can affect the local concentration of microbubbles, how they interact with the ultrasound field [114], and, more importantly, how much drug will be delivered to the brain [79]. Unfortunately, many of these parameters are difficult to predict and are expected to vary significantly across different patients and diseases. Thus, methods are needed to (i) determine what parameters to use (treatment planning), (ii) refine them during sonication to ensure BBB disruption without overexposure (treatment monitoring), and (iii) evaluate the treatment effects (treatment evaluation).

4.6.1 Treatment planning—In most cases, experiments evaluating FUS-induced BBB disruption in animal models have used a fixed set of acoustic parameters determined from prior experience and simple, geometrically-focused transducers. In general, accurate targeting can be achieved with such systems using stereotactic frames [165] if image-guidance is not available, and fairly repeatable results can be obtained with sonication through the thin skull in mice and rats, or in larger animals through a craniotomy. Methods to avoid standing waves [81] and that take into account variations in skull thickness [166] can improve repeatability in small animal studies where transcranial sonication is used.

Such approaches may be challenging to translate to human subjects, where the thicker skull is complex (a layer of trabecular bone surrounded by layers of cortical bone) and can vary substantially between individuals (3.5–9.5 mm [167]). The skull, which has a substantially higher acoustic impedance than soft tissue, will reflect most of the ultrasound beam, and the amount transmitted will depend strongly on the angle between the bone and the face of the transducer [168]. Its irregular shape can also deflect and distort the beam, and reflections within the skull cavity need to be taken into account. To correct for beam-aberrations introduced by thick skulls, phased arrays composed of more than 1000 elements combined with skull aberration correction algorithms that utilize CT data are employed [57,58]. These arrays can also be programmed to rapidly steer the beam electronically to multiple targets enabling coverage of tissue volumes [79], and different portions of the array can be disabled to reduce internal reflections or exclude certain structures.

While these approaches that use acoustic simulations and CT scans are effective in restoring the focusing of the array after transmission through the skull, clinical experience with them for thermal ablation have shown that one still needs to correct for small errors (~1–2 mm) in targeting [60,63]. To achieve this correction, one needs to be able to visualize the focal region at exposure levels that do not induce damage or other unwanted effects. Currently, this can be achieved using MRI-based methods that can visualize low-level (1–2°C) focal heating [59,169] or map small tissue displacements of a few microns induced by radiation force [170].

Ensuring accurate targeting will be most important if one aims to precisely disrupt the BBB at discrete locations. In addition, since the strength of the total microbubble activity, as well as magnitude of the disruption will depend on the vascularity of the targeted tissue (gray vs. white matter, for example [79]), it will be important to know exactly where the target is located. It might also be desirable to avoid direct sonication on large blood vessels. If one is uncertain about the targeting of the focal region, it may be challenging to understand whether a poor or unexpected result is due to an incorrect exposure level or to mistargeting. Pre-treatment imaging delineating vascularity, perfusion, or other vascular properties may prove useful for planning the treatment. It may also be useful to combine these measurements with models of the microbubble oscillations within the microvasculature [114,171].

Accurate control of the focal pressure is critical to ensure BBB disruption is produced while preventing inertial cavitation. The thick and complex human skull makes accurate focal pressure estimations extremely challenging. While the acoustic modeling methods developed for aberration correction may provide estimates of the focal pressure amplitude, it has not been validated to our knowledge. It may be possible to use the MRI-based methods mentioned above that can visualize focal displacements or heating to ensure a predictable focal pressure amplitude. Marty et al., for example, used MR acoustic radiation force imaging to ensure a consistent exposure level between subjects in BBB disruption experiments in rats [115]. However, one needs to take the underlying tissue properties (which may be unknown for tumors or other abnormalities) into account or test it in proximal normal brain locations.

4.6.2 Treatment monitoring and control—Given the challenges in predicting the focal pressure amplitude when sonicating transcranially, we anticipate that effective monitoring of the procedure will be important if this technology is to be translated to clinical use. At minimum, such monitoring should provide an indication that the exposure level is sufficient to induce BBB disruption and alert the user if inertial cavitation is occurring. One could use MRI methods for this purpose. Contrast-enhanced imaging can be used to visualize when the disruption occurs, and T2*-weighted or susceptibility-weighted MRI can be used to detect petechiae produced by inertial cavitation [77,119]. These methods could be used now for control over the procedure in initial clinical tests of FUS-induced BBB disruption with experienced users. However, performing multiple MRI acquisitions would be time-consuming and might require excessive amounts of both ultrasound and MRI contrast agents. Real-time and, perhaps, more direct methods are likely necessary for widespread clinical implementation.

For real-time monitoring and control, a number of studies have investigated the use of piezoelectric receivers operated in passive mode (i.e. only listening) to record and analyze the diverging pressure waves (i.e. acoustic emissions) emitted by oscillating microbubbles during FUS-induced BBB disruption [105–107,172,173]. The spectral content and strength of the recorded emissions is sufficient to characterize and subsequently control the microbubble oscillations. Inertial cavitation is manifested in the frequency domain of the acoustic emission as a broadband signal [53], and has generally been associated with the production of vascular damage during BBB disruption [105,107], although other studies have suggested that it can occur without damage [106]. Harmonic and/or sub- and ultra-harmonic acoustic emissions in the absence of broadband signal are indicative of stable volumetric oscillations, which consistently have been associated with safe BBB disruption [105–107]. Therefore, depending on the spectral content and strength of the emissions the output of the device can be increased until strong harmonic, subharmonic, or ultraharmonic emissions are observed, and decreased if broadband emissions are detected. O'Reilly et al. demonstrated a closed-loop controller built around the detection of ultraharmonic emissions to automatically select an acoustic exposure that could produce BBB disruption with little or no petechiae [173]. We have been exploring the strength of the harmonic emissions as a basis for such a controller, as we have found that we can reliably detect it before inertial cavitation occurs and that it is correlated with the magnitude of the BBB disruption measured via MRI contrast enhancement [105,107]. An example of this correlation observed during transcranial BBB disruption in macaques using a clinical brain FUS system is shown in Figure 9A.

If one can integrate a large number of receivers into the FUS system, one can use passive reconstruction methods [174,175] to create two- or even three-dimensional maps of the microbubble activity to ensure that it is occurring at the expected location. Examples from experiments in our laboratory in macaques using a linear receiver array integrated into a clinical brain FUS system are shown in Figure 9B–C. In these experiments, we found that the cavitation activity in the passive acoustic maps (red area in Figure 9B–C) was co-localized with the resulting BBB disruption [176].

4.6.3 Treatment evaluation—As described above, contrast-enhanced imaging and T2*- or susceptibility-weighted imaging can be used to verify that BBB disruption has occurred and whether significant vascular damage has occurred, respectively. For tumors, it may be necessary to compare the signal enhancement after contrast injection to measurements obtained before FUS. Other imaging modalities may also be useful [177]. If the contrast-enhanced imaging is obtained before the therapeutic agent is injected, one can confirm that the BBB disruption is only occurring at the targeted locations before administering the drug, providing another level of control to ensure that drugs are delivered only to desired regions.

Post-treatment imaging could be more useful if one could use it to estimate drug uptake and penetration in the brain. This can be achieved directly by labeling the drug with a contrast agent for MRI or other modality [146]. It might also be possible to use a standard contrast agent as a surrogate measurement. A number of studies have related signal intensity changes of contrast-enhanced MRI at the end of the sonication with tissue drug concentrations [83,147,178]. More quantitative and repeatable techniques, such as estimating contrast agent

concentrations via T1-mapping [115,179] or vascular transfer coefficients via analysis of dynamic contrast-enhanced MRI (DCE-MRI) [180] have been used to perform spatial and temporal characterization of BBB permeability. DCE-MRI can also predict the resulting payload of drugs to the brain [96] and in some cases, in tumors [179]. Examples showing DCE-MRI evaluation of BBB disruption and its subsequent restoration over time, and its relationship to concentrations of doxorubicin are shown in Figure 10. If one understands the relationship between the concentrations of the therapeutic and the imaging contrast agent, which can perhaps be established in animals, one might be able to titrate the drug administration to achieve a desired level in the brain. However, this may be challenging in tumors, where the vascular permeability can change over time [179].

5. Going forward

Based on the extensive preclinical experience described above, along with recent studies in nonhuman primates [79,80] demonstrating that the method can be “scaled up” without producing evident tissue damage or functional deficits even after repeated sessions [79], this method for targeted drug delivery in the brain is ready in our view for initial safety tests in humans, where it will hopefully reveal its enormous potential. Clinical transcranial MRI-guided FUS systems [60,63] and commercially-available ultrasound contrast agents are available and can be used for these tests. Given the huge clinical need and the existence of available approved anticancer agents that are expected to be effective if they could be adequately delivered, brain tumors may be an appropriate target for these initial tests.

Given MRI's high cost and complexity, coupled with the need in many cases to administer therapeutics over multiple sessions, it would be desirable in the long run to develop systems to provide FUS-induced BBB outside of the MRI environment. Passive cavitation monitoring and/or mapping may be the enabling technology for this translation away from MRI guidance. One can envision systems that use pre-treatment MRI and CT (to delineate different tissue structures and skull density, respectively), along with “frameless” navigation and cavitation monitoring to provide routine BBB disruption in an outpatient facility. A number of technical developments, such as reducing targeting error during transcranial sonication, finding methods to easily register the position of the skull within the FUS device without a stereotactic frame, and developing methods to better quantify acoustic emissions measurements obtained through the thicker human skull, are needed to reach this goal. In our opinion, all of these things are achievable. It would also be desirable to remove the need to shave the head, which is currently needed to allow for acoustic coupling. Attenuation should not prevent this [181].

The potential of this technique to manipulate the amount of drug delivered to each point in the brain can provide a level of control that is not readily available with existing technologies. This control can be achieved by modulating the acoustic parameters to control the “level” of the disruption, by analyzing the post-sonication contrast enhancement before injecting the drug and titrating the drug dose, or by repeating sonication at select areas after some delay to lengthen the time the barrier is disrupted [96]. It might even be possible to tailor the sonication parameters and BBB disruption to the molecular weight of the therapeutic agent. These methods may enable “dose painting” that can give clinicians new

flexibility in how drugs are used in the CNS to maximize efficacy and minimizing side effects. Further targeting and control can be achieved by loading drugs into microbubbles [146,152–155] or by using magnetic targeting after FUS-induced BBB disruption [144–146].

It will also be important to establish the feasibility and safety of targeting very large volumes. Many promising applications of this technology (brain tumors, Alzheimer's disease, etc.) will require sonication over large portions of the brain for greatest effect. This can be achieved by systematically focusing the ultrasound beam to a large number of individual targets. It should be possible to target the hundreds or thousands of focal points needed to achieve such large-scale BBB disruption in a reasonable amount of time. Given the low duty cycle and minimal acoustic exposure levels needed to induce the effect, many targets can be sonicated simultaneously. For example, with the low duty cycle needed to induce BBB disruption (1% or less), we can target 100 targets or more with electronic beam steering with a phased array in the same amount of time it currently takes to disrupt one location with the simple system we use for small animal experiments. While again this will require technical improvements and more safety tests, we expect that achieving controlled, large volume BBB disruption is achievable.

It would be helpful if the physical and/or physiological mechanisms by which the mechanical effects of FUS and microbubbles induce BBB disruption were elucidated. Without knowledge of the mechanism, one can only speculate on how one can optimize the procedure, and we are left with performing time-consuming parametric studies. Given the large parameter space in variables that can influence the magnitude of the BBB disruption, it is possible that we have not stumbled upon parameters that can further improve upon the safe window where BBB disruption is possible. Multidisciplinary approaches are very likely to prove fruitful and could potentially identify a unique physiologic mechanism, perhaps with interesting implications on the structure and function of the vasculature in the CNS.

Other tissues have barriers similar to the BBB and could benefit from similar microbubble-enhanced sonications or prove to be simpler models to study the aforementioned interactions. There is data demonstrating that disruption of the blood-retinal [182] and blood-spinal cord [183] barriers can be disrupted by FUS, and that the glomerular function in the kidney can be enhanced, presumably through changes in the “blood-urine barrier” [184]. Also, using pressure amplitudes higher than are needed for FUS-induced BBB disruption, one can use microbubble-enhanced sonications for ablation [185], thrombolysis [186], or radiosensitization [187]. One can potentially combine one of these microbubble-enhanced therapies with BBB disruption to produce a synergistic effect or to deliver therapeutics in the surrounding tissues.

The clinical need for new approaches to bypass the BBB in order to increase the number of drugs that can be used effectively in the CNS is tremendous. In addition to CNS disorders such as brain tumors, stroke, trauma, and genetic neurodegenerative disorders, opportunities may exist for a wide range of other applications. Examples include pain management, and psychological disorders such as addiction, both of which may benefit from a technology that permits drug transport to precise targets in the brain. Existing drugs for these conditions can

have severe side effects that limit their use. With an ever-growing knowledge of brain function and dysfunction, precise drug targeting in the CNS may prove to be particularly important. Technical improvements that are achievable in our view could enable FUS to be used on a wide scale for routine targeted drug delivery to the CNS.

6. Conclusion

FUS is a unique technology that can induce BBB or BTB permeabilization that is targeted, noninvasive and transient. Extensive work in preclinical studies has demonstrated that it can enable the delivery of therapeutics that normally do not reach the brain, and enhance their delivery to brain tumors. The sonications do not appear to have any deleterious effects on the brain, and the method is readily repeatable. MRI and acoustic methods to plan, monitor, and evaluate the treatment offer the possibility of having control over where drugs are delivered and in what concentration. Given the availability of clinical FUS devices capable of focusing ultrasound through the intact human skull, along with recent safety studies demonstrating the method can be performed safely in nonhuman primates, it appears that the method is ready for initial clinical tests.

Acknowledgments

Support: This work was supported by NIH grants P01CA174645, P41EB015898, P41RR019703, R25CA089017.

8. Reference List

[1]. Neuwelt EA, Bauer B, Fahlke C, Fricker G, Iadecola C, Janigro D, Leybaert L, Molnar Z, O'Donnell ME, Povlishock JT, Saunders NR, Sharp F, Stanimirovic D, Watts RJ, Drewes LR. Engaging neuroscience to advance translational research in brain barrier biology. Nat Rev Neurosci. 2011; 12:169–182. [PubMed: 21331083]

[2]. Abbott NJ, Romero IA. Transporting therapeutics across the blood-brain barrier. Mol. Med Today. 1996; 2:106–113. [PubMed: 8796867]

[3]. Pardridge WM. Molecular biology of the blood-brain barrier. Mol. Biotechnol. 2005; 30:57–70. [PubMed: 15805577]

[4]. Eichler AF, Chung E, Kodack DP, Loeffler JS, Fukumura D, Jain RK. The biology of brain metastases-translation to new therapies. Nat Rev Clin Oncol. 2011; 8:344–356. [PubMed: 21487419]

[5]. Minniti G, Amelio D, Amichetti M, Salvati M, Muni R, Bozzao A, Lanzetta G, Scarpino S, Arcella A, Enrici RM. Patterns of failure and comparison of different target volume delineations in patients with glioblastoma treated with conformal radiotherapy plus concomitant and adjuvant temozolomide. Radiother. Oncol. 2010; 97:377–381. [PubMed: 20855119]

[6]. Dobelbower MC, Burnett OL Iii, Nordal RA, Nabors LB, Markert JM, Hyatt MD, Fiveash JB. Patterns of failure for glioblastoma multiforme following concurrent radiation and temozolomide. J Med Imaging Radiat. Oncol. 2011; 55:77–81. [PubMed: 21382192]

[7]. Chamberlain MC. Radiographic patterns of relapse in glioblastoma. J Neurooncol. 2011; 101:319–323. [PubMed: 21052776]

[8]. Fukumura D, Jain RK. Tumor microenvironment abnormalities: causes, consequences, and strategies to normalize. J Cell Biochem. 2007; 101:937–949. [PubMed: 17171643]

[9]. Regina A, Demeule M, Laplante A, Jodoin J, Dagenais C, Berthelet F, Moghrabi A, Beliveau R. Multidrug resistance in brain tumors: roles of the blood-brain barrier. Cancer etastasis Rev. 2001; 20:13–25.

[10]. Lockman PR, Mittapalli RK, Taskar KS, Rudraraju V, Gril B, Bohn KA, Adkins CE, Roberts A, Thorsheim HR, Gaasch JA, Huang S, Palmieri D, Steeg PS, Smith QR. Heterogeneous blood-

tumor barrier permeability determines drug efficacy in experimental brain metastases of breast cancer. Clin Cancer Res. 2010; 16:5664–5678. [PubMed: 20829328]

[11]. Groothuis DR. The blood-brain and blood-tumor barriers: a review of strategies for increasing drug delivery. Neuro. -oncol. 2000; 2:45–59. [PubMed: 11302254]

[12]. Pardridge WM. Blood-brain barrier delivery. Drug Discov. Today. 2007; 12:54–61. [PubMed: 17198973]

[13]. Blumling JP Iii, Silva GA. Targeting the brain: advances in drug delivery. Curr Pharm Biotechnol. 2012; 13:2417–2426. [PubMed: 23016646]

[14]. Tomita T. Interstitial chemotherapy for brain tumors: review. J Neurooncol. 1991; 10:57–74. [PubMed: 2022973]

[15]. Bobo RH, Laske DW, Akbasak A, Morrison PF, Dedrick RL, Oldfield EH. Convection-enhanced delivery of macromolecules in the brain. Proc. Natl. Acad. Sci. U. S. A. 1994; 91:2076–2080. [PubMed: 8134351]

[16]. Guerin C, Olivi A, Weingart JD, Lawson HC, Brem H. Recent advances in brain tumor therapy: local intracerebral drug delivery by polymers. Invest New Drugs. 2004; 22:27–37. [PubMed: 14707492]

[17]. Brem H, Gabikian P. Biodegradable polymer implants to treat brain tumors. J Control Release. 2001; 74:63–67. [PubMed: 11489483]

[18]. Fung LK, Shin M, Tyler B, Brem H, Saltzman WM. Chemotherapeutic drugs released from polymers: distribution of 1,3-bis(2-chloroethyl)-1-nitrosourea in the rat brain. Pharm Res. 1996; 13:671–682. [PubMed: 8860421]

[19]. Voges J, Reszka R, Gossmann A, Dittmar C, Richter R, Garlip G, Kracht L, Coenen HH, Sturm V, Wienhard K, Heiss WD, Jacobs AH. Imaging-guided convection-enhanced delivery and gene therapy of glioblastoma. Ann. Neurol. 2003; 54:479–487. [PubMed: 14520660]

[20]. Fleischhack G, Jaehde U, Bode U. Pharmacokinetics following intraventricular administration of chemotherapy in patients with neoplastic meningitis. Clin Pharmacokinet. 2005; 44:1–31. [PubMed: 15634030]

[21]. Illum L. Nasal drug delivery--possibilities, problems and solutions. J Control Release. 2003; 87:187–198. [PubMed: 12618035]

[22]. Illum L. Nasal drug delivery: new developments and strategies. Drug Discov. Today. 2002; 7:1184–1189. [PubMed: 12547019]

[23]. Ugwoke MI, Agu RU, Verbeke N, Kinget R. Nasal mucoadhesive drug delivery: background, applications, trends and future perspectives. Adv. Drug Deliv. Rev. 2005; 57:1640–1665. [PubMed: 16182408]

[24]. Pires A, Fortuna A, Alves G, Falcao A. Intranasal drug delivery: how, why and what for? J Pharm Pharm Sci. 2009; 12:288–311. [PubMed: 20067706]

[25]. Oldendorf WH, Hyman S, Braun L, Oldendorf SZ. Blood-brain barrier: penetration of morphine, codeine, heroin, and methadone after carotid injection. Science. 1972; 178:984–986. [PubMed: 5084666]

[26]. Abbott NJ, Patabendige AA, Dolman DE, Yusof SR, Begley DJ. Structure and function of the blood-brain barrier. Neurobiol. Dis. 2010; 37:13–25. [PubMed: 19664713]

[27]. Zhang EY, Knipp GT, Ekins S, Swaan PW. Structural biology and function of solute transporters: implications for identifying and designing substrates. Drug Metab Rev. 2002; 34:709–750. [PubMed: 12487148]

[28]. Pardridge WM. Blood-brain barrier drug targeting: the future of brain drug development. Mol. Interv. 2003; 3:90–105. 51. [PubMed: 14993430]

[29]. Pardridge WM. Drug targeting to the brain. Pharm Res. 2007; 24:1733–1744. [PubMed: 17554607]

[30]. Blasi P, Giovagnoli S, Schoubben A, Ricci M, Rossi C. Solid lipid nanoparticles for targeted brain drug delivery. Adv. Drug Deliv. Rev. 2007; 59:454–477. [PubMed: 17570559]

[31]. Olivier JC. Drug transport to brain with targeted nanoparticles. NeuroRx. 2005; 2:108–119. [PubMed: 15717062]

[32]. Schnyder A, Huwyler J. Drug transport to brain with targeted liposomes. NeuroRx. 2005; 2:99–107. [PubMed: 15717061]

[33]. Broadwell RD, Balin BJ, Salcman M. Transcytotic pathway for blood-borne protein through the blood-brain barrier. Proc Natl. Acad. Sci. U. S. A. 1988; 85:632–636. [PubMed: 2448779]

[34]. Mellman I. Endocytosis and molecular sorting. Annu. Rev Cell Dev. Biol. 1996; 12:575–625. [PubMed: 8970738]

[35]. Mukherjee S, Ghosh RN, Maxfield FR. Endocytosis. Physiol Rev. 1997; 77:759–803. [PubMed: 9234965]

[36]. Rapoport SI. Effect of concentrated solutions on blood-brain barrier. Am J Physiol. 1970; 219:270–274. [PubMed: 5424853]

[37]. Rapoport SI. Advances in osmotic opening of the blood-brain barrier to enhance CNS chemotherapy. Expert. Opin. Investig. Drugs. 2001; 10:1809–1818.

[38]. Kroll RA, Neuwelt EA. Outwitting the blood-brain barrier for therapeutic purposes: osmotic opening and other means. Neurosurgery. 1998; 42:1083–1099. [PubMed: 9588554]

[39]. Bellavance MA, Blanchette M, Fortin D. Recent advances in blood-brain barrier disruption as a CNS delivery strategy. AAPS. J. 2008; 10:166–177. [PubMed: 18446517]

[40]. Doolittle ND, Miner ME, Hall WA, Siegal T, Jerome E, Osztie E, McAllister LD, Bubalo JS, Kraemer DF, Fortin D, Nixon R, Muldoon LL, Neuwelt EA. Safety and efficacy of a multicenter study using intraarterial chemotherapy in conjunction with osmotic opening of the blood-brain barrier for the treatment of patients with malignant brain tumors. Cancer. 2000; 88:637–647. [PubMed: 10649259]

[41]. Hall WA, Doolittle ND, Daman M, Bruns PK, Muldoon L, Fortin D, Neuwelt EA. Osmotic blood-brain barrier disruption chemotherapy for diffuse pontine gliomas. J Neurooncol. 2006; 77:279–284. [PubMed: 16314949]

[42]. Jahnke K, Kraemer DF, Knight KR, Fortin D, Bell S, Doolittle ND, Muldoon LL, Neuwelt EA. Intraarterial chemotherapy and osmotic blood-brain barrier disruption for patients with embryonal and germ cell tumors of the central nervous system. Cancer. 2008; 112:581–588. [PubMed: 18072268]

[43]. Angelov L, Doolittle ND, Kraemer DF, Siegal T, Barnett GH, Peereboom DM, Stevens G, McGregor J, Jahnke K, Lacy CA, Hedrick NA, Shalom E, Ference S, Bell S, Sorenson L, Tyson RM, Haluska M, Neuwelt EA. Blood-brain barrier disruption and intra-arterial methotrexate-based therapy for newly diagnosed primary CNS lymphoma: a multi-institutional experience. J Clin Oncol. 2009; 27:3503–3509. [PubMed: 19451444]

[44]. Boockvar JA, Tsiouris AJ, Hofstetter CP, Kovanlikaya I, Fralin S, Kesavabhotla K, Seedial SM, Pannullo SC, Schwartz TH, Stieg P, Zimmerman RD, Knopman J, Scheff RJ, Christos P, Vallabhajosula S, Riina HA. Safety and maximum tolerated dose of superselective intraarterial cerebral infusion of bevacizumab after osmotic blood-brain barrier disruption for recurrent malignant glioma. Clinical article. J Neurosurg. 2011; 114:624–632. [PubMed: 20964595]

[45]. Guillaume DJ, Doolittle ND, Gahramanov S, Hedrick NA, Delashaw JB, Neuwelt EA. Intra-arterial chemotherapy with osmotic blood-brain barrier disruption for aggressive oligodendroglial tumors: results of a phase I study. Neurosurgery. 2010; 66:48–58. [PubMed: 20023537]

[46]. Inamura T, Nomura T, Ikezaki K, Fukui M, Pollinger G, Black KL. Intracarotid histamine infusion increases blood tumour permeability in RG2 glioma. Neurol. Res. 1994; 16:125–128. [PubMed: 7913997]

[47]. Gutman M, Laufer R, Eisenthal A, Goldman G, Ravid A, Inbar M, Klausner JM. Increased microvascular permeability induced by prolonged interleukin-2 administration is attenuated by the oxygen-free-radical scavenger dimethylthiourea. Cancer Immunol. Immunother. 1996; 43:240–244. [PubMed: 9003470]

[48]. Black KL, Chio CC. Increased opening of blood-tumour barrier by leukotriene C4 is dependent on size of molecules. Neurol Res. 1992; 14:402–404. [PubMed: 1282688]

[49]. de Vries HE, Blom-Roosemalen MC, van Oosten M, de Boer AG, van Berkel TJ, Breimer DD, Kuiper J. The influence of cytokines on the integrity of the blood-brain barrier in vitro. J Neuroimmunol. 1996; 64:37–43. [PubMed: 8598388]

[50]. Lynn JG, Putnam TJ. Histology of cerebral lesions produced by focused ultrasound. Am. J. Path. 1944; 20:637–652. [PubMed: 19970769]

[51]. Fry WJ, Fry FJ. Fundamental neurological research and human neurosurgery using intense ultrasound. IRE Trans. Med. Electron. 1960; ME-7:166–181. [PubMed: 13702332]

[52]. Ballantine HT, Bell E, Manlapaz J. Progress and problems in the neurological applications of focused ultrasound. J. Neurosurg. 1960; 17:858–876. [PubMed: 13686380]

[53]. Lele, PP. Effects of ultrasound on “solid” mammalian tissues and tumors in vivo. In: Repacholi, MH.; Grondolfo, M.; Rindi, A., editors. Ultrasound: Medical Applications, Biological Effects and Hazard Potential. Plenum Pub. Corp.; New York: 1987. p. 275-306.

[54]. Meyers R, Fry WJ, Fry FJ, Dreyer LL, Shultz DF, Noyes RF. Early experiences with ultrasonic irradiation of the pallidfugal and nigral complexes in hyperkinetic and hypertonic disorders. J. Neurosurg. 1959; 16:32–54. [PubMed: 13621264]

[55]. Heimburger RF. Ultrasound augmentation of central nervous system tumor therapy. Indiana. Med. 1985; 78:469–476. [PubMed: 4020091]

[56]. Hynynen K, McDannold N. MRI guided and monitored focused ultrasound thermal ablation methods: a review of progress. Int. J. Hyperthermia. 2004; 20:725–737. [PubMed: 15675668]

[57]. Clement GT, Hynynen K. A non-invasive method for focusing ultrasound through the human skull. Phys. Med. Biol. 2002; 47:1219–1236. [PubMed: 12030552]

[58]. Aubry JF, Tanter M, Pernot M, Thomas JL, Fink M. Experimental demonstration of noninvasive transskull adaptive focusing based on prior computed tomography scans. J. Acoust. Soc. Am. 2003; 113:84–93. [PubMed: 12558249]

[59]. Ishihara Y, Calderon A, Watanabe H, Okamoto K, Suzuki Y, Kuroda K. A precise and fast temperature mapping using water proton chemical shift. Magn. Reson. Med. 1995; 34:814–823. [PubMed: 8598808]

[60]. McDannold N, Clement GT, Black P, Jolesz F, Hynynen K. Transcranial magnetic resonance imaging- guided focused ultrasound surgery of brain tumors: initial findings in 3 patients. Neurosurgery. 2010; 66:323–332. [PubMed: 20087132]

[61]. Lipsman N, Schwartz ML, Huang Y, Lee L, Sankar T, Chapman M, Hynynen K, Lozano AM. MR-guided focused ultrasound thalamotomy for essential tremor: a proof-of-concept study. Lancet Neurol. 2013; 12:462–468. [PubMed: 23523144]

[62]. Elias WJ, Huss D, Voss T, Loomba J, Khaled M, Zadicario E, Frysinger RC, Sperling SA, Wylie S, Monteith SJ, Druzgal J, Shah BB, Harrison M, Wintermark M. A pilot study of focused ultrasound thalamotomy for essential tremor. N. Engl. J. Med. 2013; 369:640–648. [PubMed: 23944301]

[63]. Martin E, Jeanmonod D, Morel A, Zadicario E, Werner B. High-intensity focused ultrasound for noninvasive functional neurosurgery. Ann. Neurol. 2009; 66:858–861. [PubMed: 20033983]

[64]. Nyborg, WL.; Carson, PL.; Carstensen, EL.; Dunn, F.; Miller, DL.; Miller, MW.; Thompson, HE.; Ziskin, MC.; Apfel, RE.; Church, CC.; Crum, LA. Criteria based on all known mechanisms (NCRP Report No. 140). National Council on Radiation Protection and Measurements; Bethesda, Maryland: 2002. Exposure criteria for medical diagnostic ultrasound: II.

[65]. Leighton, TG. The Acoustic Bubble. Academic Press Limited; San Diego, CA: 1994.

[66]. Dayton P, Klibanov A, Brandenburger G, Ferrara K. Acoustic radiation force in vivo: a mechanism to assist targeting of microbubbles. Ultrasound Med Biol. 1999; 25:1195–1201. [PubMed: 10576262]

[67]. Miller DL. Particle gathering and microstreaming near ultrasonically activated gas-filled micropores. J. Acoust. Soc. Am. 1988; 84:1378–1387. [PubMed: 3198872]

[68]. Edmonds PD, Sancier KM. Evidence for free radical production by ultrasonic cavitation in biological media. Ultrasound Med. Biol. 1983; 9:635–639. [PubMed: 6322402]

[69]. Flynn HG. Generation of transient cavities in liquids by microsecond pulses of ultrasound. J. Acoust. Soc. Am. 1982; 72:1926–1932.

[70]. Apfel RE. Acoustic cavitation: a possible consequence of biomedical uses of ultrasound. Br. J. Cancer Suppl. 1982; 45:140–146. [PubMed: 6950749]

[71]. Bakay L, Hueter TF, Ballantine HT, Sosa D. Ultrasonically produced changes in the blood-brain barrier. Arch. Neurol. 1956; 76:457–467.

[72]. Vykhodtseva, N. Effects of high intensity pulsed ultrasound on brain tissues. The 5th International Symposium on Ultrasound in Biol Med.; Puschino, Russia. 1981. p. 95-97.

[73]. Patrick JT, Nolting MN, Goss SA, Dines KA, Clendenon JL, Rea MA, Heimburger RF. Ultrasound and the blood-brain barrier. Adv. Exp. Med. Biol. 1990; 267:369–381. [PubMed: 2088054]

[74]. Vykhodtseva NI, Hynynen K, Damianou C. Histologic effects of high intensity pulsed ultrasound exposure with subharmonic emission in rabbit brain in vivo. Ultrasound Med. Biol. 1995; 21:969–979. [PubMed: 7491751]

[75]. Mesiwala AH, Farrell L, Wenzel HJ, Silbergeld DL, Crum LA, Winn HR, Mourad PD. High-intensity focused ultrasound selectively disrupts the blood-brain barrier in vivo. Ultrasound Med. Biol. 2002; 28:389–400. [PubMed: 11978420]

[76]. McDannold N, Vykhodtseva N, Jolesz FA, Hynynen K. MRI investigation of the threshold for thermally induced blood-brain barrier disruption and brain tissue damage in the rabbit brain. Magn. Reson. Med. 2004; 51:913–923. [PubMed: 15122673]

[77]. Hynynen K, McDannold N, Vykhodtseva N, Jolesz FA. Noninvasive MR imaging-guided focal opening of the blood-brain barrier in rabbits. Radiology. 2001; 220:640–646. [PubMed: 11526261]

[78]. Sheikov N, McDannold N, Vykhodtseva N, Jolesz F, Hynynen K. Cellular mechanisms of the blood-brain barrier opening induced by ultrasound in presence of microbubbles. Ultrasound Med. Biol. 2004; 30:979–989. [PubMed: 15313330]

[79]. McDannold N, Arvanitis CD, Vykhodtseva N, Livingstone MS. Temporary disruption of the blood-brain barrier by use of ultrasound and microbubbles: safety and efficacy evaluation in rhesus macaques. Cancer Res. 2012; 72:3652–3663. [PubMed: 22552291]

[80]. Marquet F, Tung YS, Teichert T, Ferrera VP, Konofagou EE. Noninvasive, transient and selective blood-brain barrier opening in non-human primates in vivo. PLoS One. 2011; 6:e22598. [PubMed: 21799913]

[81]. O'Reilly MA, Huang Y, Hynynen K. The impact of standing wave effects on transcranial focused ultrasound disruption of the blood-brain barrier in a rat model. Phys Med Biol. 2010; 55:5251–5267. [PubMed: 20720286]

[82]. Hynynen K, McDannold N, Sheikov NA, Jolesz FA, Vykhodtseva N. Local and reversible blood-brain barrier disruption by noninvasive focused ultrasound at frequencies suitable for trans-skull sonications. Neuroimage. 2005; 24:12–20. [PubMed: 15588592]

[83]. Treat LH, McDannold N, Zhang Y, Vykhodtseva N, Hynynen K. Targeted delivery of doxorubicin to the rat brain at therapeutic levels using MRI-guided focused ultrasound. Int. J. Cancer. 2007; 121:901–907. [PubMed: 17437269]

[84]. Chopra R, Vykhodtseva N, Hynynen K. Influence of exposure time and pressure amplitude on blood-brain-barrier opening using transcranial ultrasound exposures. ACS Chem. Neurosci. 2010; 1:391–398. [PubMed: 20563295]

[85]. McDannold N, Vykhodtseva N, Hynynen K. Blood-brain barrier disruption induced by focused ultrasound and circulating preformed microbubbles appears to be characterized by the mechanical index. Ultrasound Med. Biol. 2008; 34:834–840. [PubMed: 18207311]

[86]. McDannold N, Vykhodtseva N, Hynynen K. Effects of Acoustic Parameters and Ultrasound Contrast Agent Dose on Focused-Ultrasound Induced Blood-Brain Barrier Disruption. Ultrasound Med. Biol. 2008; 34:930–937. [PubMed: 18294757]

[87]. Choi JJ, Feshitan JA, Baseri B, Wang S, Tung YS, Borden MA, Konofagou EE. Microbubble-size dependence of focused ultrasound-induced blood-brain barrier opening in mice in vivo. IEEE Trans. Biomed. Eng. 2010; 57:145–154. [PubMed: 19846365]

[88]. Vlachos F, Tung YS, Konofagou E. Permeability dependence study of the focused ultrasound-induced blood-brain barrier opening at distinct pressures and microbubble diameters using DCE-MRI. Magn Reson. Med. 2011; 66:821–830. [PubMed: 21465543]

[89]. Samiotaki G, Vlachos F, Tung YS, Konofagou EE. A quantitative pressure and microbubble-size dependence study of focused ultrasound-induced blood-brain barrier opening reversibility in vivo using MRI. Magn Reson. Med. 2012; 67:769–777. [PubMed: 21858862]

[90]. Choi JJ, Selert K, Gao Z, Samiotaki G, Baseri B, Konofagou EE. Noninvasive and localized blood-brain barrier disruption using focused ultrasound can be achieved at short pulse lengths and low pulse repetition frequencies. J Cereb. Blood Flow Metab. 2011; 31:725–737. [PubMed: 20842160]

[91]. Choi JJ, Selert K, Vlachos F, Wong A, Konofagou EE. Noninvasive and localized neuronal delivery using short ultrasonic pulses and microbubbles. Proc Natl. Acad. Sci. U. S. A. 2011; 108:16539–16544. [PubMed: 21930942]

[92]. Bing KF, Howles GP, Qi Y, Palmeri ML, Nightingale KR. Blood-brain barrier (BBB) disruption using a diagnostic ultrasound scanner and Definity in Mice. Ultrasound Med Biol. 2009; 35:1298–1308. [PubMed: 19545939]

[93]. Yang FY, Fu WM, Yang RS, Liou HC, Kang KH, Lin WL. Quantitative evaluation of focused ultrasound with a contrast agent on blood-brain barrier disruption. Ultrasound Med. Biol. 2007; 33:1421–1427. [PubMed: 17561334]

[94]. Weng JC, Wu SK, Lin WL, Tseng WY. Detecting blood-brain barrier disruption within minimal hemorrhage following transcranial focused ultrasound: a correlation study with contrast-enhanced MRI. Magn Reson. Med. 2011; 65:802–811. [PubMed: 20941741]

[95]. Weng JC, Wu SK, Yang FY, Lin WL, Tseng WY. Pulse sequence and timing of contrast-enhanced MRI for assessing blood-brain barrier disruption after transcranial focused ultrasound in the presence of hemorrhage. J. Magn Reson. Imaging. 2010; 31:1323–1330. [PubMed: 20512883]

[96]. Park J, Zhang Y, Vykhodtseva N, Jolesz FA, McDannold NJ. The kinetics of blood brain barrier permeability and targeted doxorubicin delivery into brain induced by focused ultrasound. J Control Release. 2012; 162:134–142. [PubMed: 22709590]

[97]. Yang FY, Lin YS, Kang KH, Chao TK. Reversible blood-brain barrier disruption by repeated transcranial focused ultrasound allows enhanced extravasation. J Control Release. 2011; 150:111–116. [PubMed: 21070825]

[98]. O'Reilly MA, Waspe AC, Ganguly M, Hynynen K. Focused-ultrasound disruption of the blood-brain barrier using closely-timed short pulses: influence of sonication parameters and injection rate. Ultrasound Med Biol. 2011; 37:587–594. [PubMed: 21376455]

[99]. McDannold N, Zhang Y, Vykhodtseva N. Blood-brain barrier disruption and vascular damage induced by ultrasound bursts combined with microbubbles can be influenced by choice of anesthesia protocol. Ultrasound Med Biol. 2011; 37:1259–1270. [PubMed: 21645965]

[100]. Wang JE, Liu YH, Liu LB, Xia CY, Zhang Z, Xue YX. Effects of combining low frequency ultrasound irradiation with papaverine on the permeability of the blood-tumor barrier. J. Neurooncol. 2010

[101]. Zhang Z, Xia C, Xue Y, Liu Y. Synergistic effect of low-frequency ultrasound and low-dose bradykinin on increasing permeability of the blood-tumor barrier by opening tight junction. J. Neurosci. Res. 2009; 87:2282–2289. [PubMed: 19326437]

[102]. Zhang Z, Xue Y, Liu Y, Shang X. Additive effect of low-frequency ultrasound and endothelial monocyte-activating polypeptide II on blood-tumor barrier in rats with brain glioma. Neurosci. Lett. 2010; 481:21–25. [PubMed: 20600613]

[103]. Goertz DE, Wright C, Hynynen K. Contrast agent kinetics in the rabbit brain during exposure to therapeutic ultrasound. Ultrasound Med Biol. 2010; 36:916–924. [PubMed: 20447757]

[104]. Liu HL, Pan CH, Ting CY, Hsiao MJ. Opening of the blood-brain barrier by low-frequency (28-kHz) ultrasound: a novel pinhole-assisted mechanical scanning device. Ultrasound Med Biol. 2010; 36:325–335. [PubMed: 20018435]

[105]. McDannold N, Vykhodtseva N, Hynynen K. Targeted disruption of the blood-brain barrier with focused ultrasound: association with cavitation activity. Phys. Med. Biol. 2006; 51:793–807. [PubMed: 16467579]

[106]. Tung YS, Vlachos F, Choi JJ, Deffieux T, Selert K, Konofagou EE. In vivo transcranial cavitation threshold detection during ultrasound-induced blood-brain barrier opening in mice. Phys Med Biol. 2010; 55:6141–6155. [PubMed: 20876972]

[107]. Arvanitis CD, Livingstone MS, Vykhodtseva N, McDannold N. Controlled ultrasound-induced blood-brain barrier disruption using passive acoustic emissions monitoring. PLoS One. 2012; 7:e45783. [PubMed: 23029240]

[108]. Deng CX, Sieling F, Pan H, Cui J. Ultrasound-induced cell membrane porosity. Ultrasound Med Biol. 2004; 30:519–526. [PubMed: 15121254]

[109]. Sheikov N, McDannold N, Sharma S, Hynynen K. Effect of focused ultrasound applied with an ultrasound contrast agent on the tight junctional integrity of the brain microvascular endothelium. Ultrasound Med. Biol. 2008; 34:1093–1104. [PubMed: 18378064]

[110]. Sheikov N, McDannold N, Jolesz F, Zhang YZ, Tam K, Hynynen K. Brain arterioles show more active vesicular transport of blood-borne tracer molecules than capillaries and venules after focused ultrasound-evoked opening of the blood-brain barrier. Ultrasound Med. Biol. 2006; 32:1399–1409. [PubMed: 16965980]

[111]. Raymond SB, Skoch J, Hynynen K, Bacskai BJ. Multiphoton imaging of ultrasound/Optison mediated cerebrovascular effects in vivo. J. Cereb. Blood Flow Metab. 2007; 27:393–403. [PubMed: 16685254]

[112]. Cho EE, Drazic J, Ganguly M, Stefanovic B, Hynynen K. Two-photon fluorescence microscopy study of cerebrovascular dynamics in ultrasound-induced blood-brain barrier opening. J Cereb. Blood Flow Metab. 2011; 31:1852–1862. [PubMed: 21505473]

[113]. Chen H, Kreider W, Brayman AA, Bailey MR, Matula TJ. Blood vessel deformations on microsecond time scales by ultrasonic cavitation. Phys Rev Lett. 2011; 106:034301. [PubMed: 21405276]

[114]. Sassaroli E, Hynynen K. Resonance frequency of microbubbles in small blood vessels: a numerical study. Phys. Med. Biol. 2005; 50:5293–5305. [PubMed: 16264254]

[115]. Marty B, Larrat B, Van Landeghem M, Robic C, Robert P, Port M, Le Bihan D, Pernot M, Tanter M, Lethimonnier F, Meriaux S. Dynamic study of blood-brain barrier closure after its disruption using ultrasound: a quantitative analysis. J Cereb. Blood Flow Metab. 2012; 32:1948–1958. [PubMed: 22805875]

[116]. Howles GP, Bing KF, Qi Y, Rosenzweig SJ, Nightingale KR, Johnson GA. Contrast-enhanced in vivo magnetic resonance microscopy of the mouse brain enabled by noninvasive opening of the blood-brain barrier with ultrasound. Magn Reson. Med. 2010; 64:995–1004. [PubMed: 20740666]

[117]. Baseri B, Choi JJ, Tung YS, Konofagou EE. Multi-modality safety assessment of blood-brain barrier opening using focused ultrasound and definity microbubbles: a short-term study. Ultrasound Med Biol. 2010; 36:1445–1459. [PubMed: 20800172]

[118]. McDannold N, Vykhodtseva N, Raymond S, Jolesz FA, Hynynen K. MRI-guided targeted blood-brain barrier disruption with focused ultrasound: Histological findings in rabbits. Ultrasound Med. Biol. 2005; 31:1527–1537. [PubMed: 16286030]

[119]. Liu HL, Wai YY, Chen WS, Chen JC, Hsu PH, Wu XY, Huang WC, Yen TC, Wang JJ. Hemorrhage detection during focused-ultrasound induced blood-brain-barrier opening by using susceptibility-weighted magnetic resonance imaging. Ultrasound Med Biol. 2008; 34:598–606. [PubMed: 18313204]

[120]. Hynynen K, McDannold N, Vykhodtseva N, Raymond S, Weissleder R, Jolesz FA, Sheikov N. Focal disruption of the blood-brain barrier due to 260-kHz ultrasound bursts: a method for molecular imaging and targeted drug delivery. J. Neurosurgery. 2006; 105:445–454.

[121]. Liu HL, Wai YY, Hsu PH, Lyu LA, Wu JS, Shen CR, Chen JC, Yen TC, Wang JJ. In vivo assessment of macrophage CNS infiltration during disruption of the blood-brain barrier with focused ultrasound: a magnetic resonance imaging study. J. Cereb. Blood Flow Metab. 2010; 30:674. [PubMed: 20195293]

[122]. Shang X, Wang P, Liu Y, Zhang Z, Xue Y. Mechanism of low-frequency ultrasound in opening blood-tumor barrier by tight junction. J Mol. Neurosci. 2011; 43:364–369. [PubMed: 20852968]

[123]. Alonso A, Reinz E, Jenne JW, Fatar M, Schmidt-Glenewinkel H, Hennerici MG, Meairs S. Reorganization of gap junctions after focused ultrasound blood-brain barrier opening in the rat brain. J. Cereb. Blood Flow Metab. 2010; 30:1394–1402. [PubMed: 20332798]

[124]. Deng J, Huang Q, Wang F, Liu Y, Wang Z, Wang Z, Zhang Q, Lei B, Cheng Y. The role of caveolin-1 in blood-brain barrier disruption induced by focused ultrasound combined with microbubbles. J Mol. Neurosci. 2012; 46:677–687. [PubMed: 21861133]

[125]. Xia CY, Liu YH, Wang P, Xue YX. Low-Frequency Ultrasound Irradiation Increases Blood-Tumor Barrier Permeability by Transcellular Pathway in a Rat Glioma Model. J Mol. Neurosci. 2012

[126]. Shajahan AN, Tiruppathi C, Smrcka AV, Malik AB, Minshall RD. Gbetagamma activation of Src induces caveolae-mediated endocytosis in endothelial cells. J Biol Chem. 2004; 279:48055–48062. [PubMed: 15345719]

[127]. Jalali S, Huang Y, Dumont DJ, Hynynen K. Focused ultrasound-mediated bbb disruption is associated with an increase in activation of AKT: experimental study in rats. BMC. Neurol. 2010; 10:114. [PubMed: 21078165]

[128]. Zhao H, Sapolsky RM, Steinberg GK. Phosphoinositide-3-kinase/akt survival signal pathways are implicated in neuronal survival after stroke. Mol. Neurobiol. 2006; 34:249–270. [PubMed: 17308356]

[129]. Nath R, McGinnis K, Dutta S, Shivers B, Wang KK. Inhibition of p38 kinase mimics survival signal-linked protection against apoptosis in rat cerebellar granule neurons. Cell Mol. Biol Lett. 2001; 6:173–184. [PubMed: 11544639]

[130]. Harada J, Sugimoto M. An inhibitor of p38 and JNK MAP kinases prevents activation of caspase and apoptosis of cultured cerebellar granule neurons. Jpn J Pharmacol. 1999; 79:369–378. [PubMed: 10230866]

[131]. Alonso A, Reinz E, Fatar M, Jenne J, Hennerici MG, Meairs S. Neurons but not glial cells overexpress ubiquitin in the rat brain following focused ultrasound-induced opening of the blood-brain barrier. Neuroscience. 2010; 169:116–124. [PubMed: 20416361]

[132]. Park J, Fan Z, Kumon RE, El Sayed ME, Deng CX. Modulation of intracellular Ca2+ concentration in brain microvascular endothelial cells in vitro by acoustic cavitation. Ultrasound Med Biol. 2010; 36:1176–1187. [PubMed: 20620704]

[133]. Park J, Fan Z, Deng CX. Effects of shear stress cultivation on cell membrane disruption and intracellular calcium concentration in sonoporation of endothelial cells. J Biomech. 2011; 44:164–169. [PubMed: 20863503]

[134]. Ayata C, Shin HK, Salomone S, Ozdemir-Gursoy Y, Boas DA, Dunn AK, Moskowitz MA. Pronounced hypoperfusion during spreading depression in mouse cortex. J Cereb. Blood Flow Metab. 2004; 24:1172–1182. [PubMed: 15529018]

[135]. Burgess A, Huang Y, Querbes W, Sah DW, Hynynen K. Focused ultrasound for targeted delivery of siRNA and efficient knockdown of Htt expression. J Control Release. 2012; 163:125–129. [PubMed: 22921802]

[136]. Choi JJ, Wang S, Tung YS, Morrison B III, Konofagou EE. Molecules of various pharmacologically-relevant sizes can cross the ultrasound-induced blood-brain barrier opening in vivo. Ultrasound Med Biol. 2010; 36:58–67. [PubMed: 19900750]

[137]. Muldoon LL, Pagel MA, Kroll RA, Roman-Goldstein S, Jones RS, Neuwelt EA. A physiological barrier distal to the anatomic blood-brain barrier in a model of transvascular delivery. AJNR. Am. J. Neuroradiol. 1999; 20:217–222. [PubMed: 10094341]

[138]. Liu HL, Hua MY, Chen PY, Chu PC, Pan CH, Yang HW, Huang CY, Wang JJ, Yen TC, Wei KC. Blood-brain barrier disruption with focused ultrasound enhances delivery of chemotherapeutic drugs for glioblastoma treatment. Radiology. 2010; 255:415–425. [PubMed: 20413754]

[139]. Mei J, Cheng Y, Song Y, Yang Y, Wang F, Liu Y, Wang Z. Experimental study on targeted methotrexate delivery to the rabbit brain via magnetic resonance imaging-guided focused ultrasound. J. Ultrasound Med. 2009; 28:871–880. [PubMed: 19546329]

[140]. Zeng HQ, Lu L, Wang F, Luo Y, Lou SF. Focused ultrasound-induced blood-brain barrier disruption enhances the delivery of cytarabine to the rat brain. J Chemother. 2012; 24:358–363. [PubMed: 23174101]

[141]. Wei KC, Chu PC, Wang HY, Huang CY, Chen PY, Tsai HC, Lu YJ, Lee PY, Tseng IC, Feng LY, Hsu PW, Yen TC, Liu HL. Focused ultrasound-induced blood-brain barrier opening to

enhance temozolomide delivery for glioblastoma treatment: a preclinical study. PLoS One. 2013; 8:e58995. [PubMed: 23527068]

[142]. Aryal M, Vykhodtseva N, Zhang YZ, Park J, McDannold N. Multiple treatments with liposomal doxorubicin and ultrasound-induced disruption of blood-tumor and blood-brain barriers improve outcomes in a rat glioma model. J Control Release. 2013; 169:103–111. [PubMed: 23603615]

[143]. Yang FY, Wong TT, Teng MC, Liu RS, Lu M, Liang HF, Wei MC. Focused ultrasound and interleukin-4 receptor-targeted liposomal doxorubicin for enhanced targeted drug delivery and antitumor effect in glioblastoma multiforme. J Control Release. 2012

[144]. Liu HL, Hua MY, Yang HW, Huang CY, Chu PC, Wu JS, Tseng IC, Wang JJ, Yen TC, Chen PY, Wei KC. Magnetic resonance monitoring of focused ultrasound/magnetic nanoparticle targeting delivery of therapeutic agents to the brain. Proc Natl. Acad. Sci. U. S. A. 2010; 107:15205–15210. [PubMed: 20696897]

[145]. Chen PY, Liu HL, Hua MY, Yang HW, Huang CY, Chu PC, Lyu LA, Tseng IC, Feng LY, Tsai HC, Chen SM, Lu YJ, Wang JJ, Yen TC, Ma YH, Wu T, Chen JP, Chuang JI, Shin JW, Hsueh C, Wei KC. Novel magnetic/ultrasound focusing system enhances nanoparticle drug delivery for glioma treatment. Neuro. Oncol. 2010; 12:1050–1060. [PubMed: 20663792]

[146]. Fan CH, Ting CY, Lin HJ, Wang CH, Liu HL, Yen TC, Yeh CK. SPIO-conjugated, doxorubicin-loaded microbubbles for concurrent MRI and focused-ultrasound enhanced brain-tumor drug delivery. Biomaterials. 2013; 34:3706–3715. [PubMed: 23433776]

[147]. Kinoshita M, McDannold N, Jolesz FA, Hynynen K. Noninvasive localized delivery of Herceptin to the mouse brain by MRI-guided focused ultrasound-induced blood-brain barrier disruption. Proc. Natl. Acad. Sci. U. S. A. 2006; 103:11719–11723. [PubMed: 16868082]

[148]. Park, EJ.; Zhang, YZ.; Vykhodtseva, N.; McDannold, N. Ultrasound-mediated blood-brain/blood-tumor barrier disruption improves outcomes with trastuzumab in a breast cancer brain metastasis model. J Control Release. 2012. http://dx.doi.org/10.1016/j.jconrel.2012.09.007

[149]. Yang FY, Chen YW, Chou FI, Yen SH, Lin YL, Wong TT. Boron neutron capture therapy for glioblastoma multiforme: enhanced drug delivery and antitumor effect following blood-brain barrier disruption induced by focused ultrasound. Future Oncol. 2012; 8:1361–1369. [PubMed: 23130933]

[150]. Alkins RD, Brodersen PM, Sodhi RN, Hynynen K. Enhancing drug delivery for boron neutron capture therapy of brain tumors with focused ultrasound. Neuro Oncol. 2013

[151]. Alkins R, Burgess A, Ganguly M, Francia G, Kerbel R, Wels WS, Hynynen K. Focused ultrasound delivers targeted immune cells to metastatic brain tumors. Cancer Res. 2013; 73:1892–1899. [PubMed: 23302230]

[152]. Ting CY, Fan CH, Liu HL, Huang CY, Hsieh HY, Yen TC, Wei KC, Yeh CK. Concurrent blood-brain barrier opening and local drug delivery using drug-carrying microbubbles and focused ultrasound for brain glioma treatment. Biomaterials. 2012; 33:704–712. [PubMed: 22019122]

[153]. Wang F, Shi Y, Lu L, Liu L, Cai Y, Zheng H, Liu X, Yan F, Zou C, Sun C, Shi J, Lu S, Chen Y. Targeted delivery of GDNF through the blood-brain barrier by MRI-guided focused ultrasound. PLoS One. 2012; 7:e52925. [PubMed: 23300823]

[154]. Huang Q, Deng J, Wang F, Chen S, Liu Y, Wang Z, Wang Z, Cheng Y. Targeted gene delivery to the mouse brain by MRI-guided focused ultrasound-induced blood-brain barrier disruption. Exp Neurol. 2012; 233:350–356. [PubMed: 22079586]

[155]. Fan CH, Ting CY, Liu HL, Huang CY, Hsieh HY, Yen TC, Wei KC, Yeh CK. Antiangiogenic-targeting drug-loaded microbubbles combined with focused ultrasound for glioma treatment. Biomaterials. 2013; 34:2142–2155. [PubMed: 23246066]

[156]. Baseri B, Choi JJ, Deffieux T, Samiotaki G, Tung YS, Olumolade O, Small SA, Morrison B, Konofagou EE. Activation of signaling pathways following localized delivery of systemically administered neurotrophic factors across the blood-brain barrier using focused ultrasound and microbubbles. Phys Med Biol. 2012; 57:N65–N81. [PubMed: 22407323]

[157]. Raymond SB, Treat LH, Dewey JD, McDannold N, Hynynen K, Bacskai BJ. Ultrasound enhanced delivery of molecular imaging and therapeutic agents in Alzheimer's disease mouse models. PLoS. ONE. 2008; 3:e2175. [PubMed: 18478109]

[158]. Jordao JF, Ayala-Grosso CA, Markham K, Huang Y, Chopra R, McLaurin J, Hynynen K, Aubert I. Antibodies targeted to the brain with image-guided focused ultrasound reduces amyloid-beta plaque load in the TgCRND8 mouse model of Alzheimer's disease. PLoS. ONE. 2010; 5:e10549. [PubMed: 20485502]

[159]. Burgess A, Ayala-Grosso CA, Ganguly M, Jordao JF, Aubert I, Hynynen K. Targeted delivery of neural stem cells to the brain using MRI-guided focused ultrasound to disrupt the blood-brain barrier. PLoS One. 2011; 6:e27877. [PubMed: 22114718]

[160]. Thevenot E, Jordao JF, O'Reilly MA, Markham K, Weng YQ, Foust KD, Kaspar BK, Hynynen K, Aubert I. Targeted delivery of self-complementary adeno-associated virus serotype 9 to the brain, using magnetic resonance imaging-guided focused ultrasound. Hum. Gene Ther. 2012; 23:1144–1155. [PubMed: 22838844]

[161]. Alonso A, Reinz E, Leuchs B, Kleinschmidt J, Fatar M, Geers B, Lentacker I, Hennerici MG, de Smedt SC, Meairs S. Focal Delivery of AAV2/1-transgenes Into the Rat Brain by Localized Ultrasound-induced BBB Opening. Mol. Ther. Nucleic Acids. 2013; 2:e73. [PubMed: 23423361]

[162]. Hsu PH, Wei KC, Huang CY, Wen CJ, Yen TC, Liu CL, Lin YT, Chen JC, Shen CR, Liu HL. Noninvasive and targeted gene delivery into the brain using microbubble-facilitated focused ultrasound. PLoS One. 2013; 8:e57682. [PubMed: 23460893]

[163]. Treat LH, McDannold N, Zhang Y, Vykhodtseva N, Hynynen K. Improved Anti-Tumor Effect of Liposomal Doxorubicin After Targeted Blood-Brain Barrier Disruption by MRI-Guided Focused Ultrasound in Rat Glioma. Ultrasound Med Biol. 2012; 38:1716–1725. [PubMed: 22818878]

[164]. Jordao JF, Thevenot E, Markham-Coultes K, Scarcelli T, Weng YQ, Xhima K, O'Reilly M, Huang Y, McLaurin J, Hynynen K, Aubert I. Amyloid-beta plaque reduction, endogenous antibody delivery and glial activation by brain-targeted, transcranial focused ultrasound. Exp Neurol. 2013

[165]. Choi JJ, Pernot M, Small SA, Konofagou EE. Noninvasive, transcranial and localized opening of the blood-brain barrier using focused ultrasound in mice. Ultrasound Med. Biol. 2007; 33:95–104. [PubMed: 17189051]

[166]. O'Reilly MA, Muller A, Hynynen K. Ultrasound insertion loss of rat parietal bone appears to be proportional to animal mass at submegahertz frequencies. Ultrasound Med Biol. 2011; 37:1930–1937. [PubMed: 21925788]

[167]. Pichardo S, Sin VW, Hynynen K. Multi-frequency characterization of the speed of sound and attenuation coefficient for longitudinal transmission of freshly excised human skulls. Phys Med Biol. 2011; 56:219–250. [PubMed: 21149950]

[168]. White PJ, Clement GT, Hynynen K. Longitudinal and shear mode ultrasound propagation in human skull bone. Ultrasound Med. Biol. 2006; 32:1085–1096. [PubMed: 16829322]

[169]. Hynynen K, Vykhodtseva NI, Chung AH, Sorrentino V, Colucci V, Jolesz FA. Thermal effects of focused ultrasound on the brain: determination with MR imaging. Radiology. 1997; 204:247–253. [PubMed: 9205255]

[170]. McDannold N, Maier SE. Magnetic resonance acoustic radiation force imaging. Med Phys. 2008; 35:3748–3758. [PubMed: 18777934]

[171]. Hosseinkhah N, Hynynen K. A three-dimensional model of an ultrasound contrast agent gas bubble and its mechanical effects on microvessels. Phys Med Biol. 2012; 57:785–808. [PubMed: 22252221]

[172]. Tung YS, Marquet F, Teichert T, Ferrera V, Konofagou EE. Feasibility of noninvasive cavitation-guided blood-brain barrier opening using focused ultrasound and microbubbles in nonhuman primates. Appl Phys Lett. 2011; 98:163704. [PubMed: 21580802]

[173]. O'Reilly MA, Hynynen K. Blood-Brain Barrier: Real-time Feedback-controlled Focused Ultrasound Disruption by Using an Acoustic Emissions-based Controller. Radiology. 2012; 263:96–106. [PubMed: 22332065]

[174]. Salgaonkar VA, Datta S, Holland CK, Mast TD. Passive cavitation imaging with ultrasound arrays. J Acoust. Soc Am. 2009; 126:3071–3083. [PubMed: 20000921]

[175]. Gyongy M, Coussios CC. Passive cavitation mapping for localization and tracking of bubble dynamics. J. Acoust. Soc Am. 2010; 128:EL175–EL180. [PubMed: 20968322]

[176]. Arvanitis CD, Livingstone MS, McDannold N. Combined ultrasound and MR imaging to guide focused ultrasound therapies in the brain. Phys Med Biol. 2013; 58:4749–4761. [PubMed: 23788054]

[177]. Yang FY, Wang HE, Lin GL, Teng MC, Lin HH, Wong TT, Liu RS. Micro-SPECT/CT-based pharmacokinetic analysis of 99mTc-diethylenetriaminepentaacetic acid in rats with blood-brain barrier disruption induced by focused ultrasound. J Nucl. Med. 2011; 52:478–484. [PubMed: 21321259]

[178]. Yang FY, Horng SC, Lin YS, Kao YH. Association between contrast-enhanced MR images and blood-brain barrier disruption following transcranial focused ultrasound. J. Magn Reson. Imaging. 2010; 32:593–599. [PubMed: 20815056]

[179]. Chu PC, Chai WY, Hsieh HY, Wang JJ, Wey SP, Huang CY, Wei KC, Liu HL. Pharmacodynamic analysis of magnetic resonance imaging-monitored focused ultrasound-induced blood-brain barrier opening for drug delivery to brain tumors. Biomed. Res Int. 2013; 2013:627496. [PubMed: 23607093]

[180]. Vlachos F, Tung YS, Konofagou EE. Permeability assessment of the focused ultrasound-induced blood-brain barrier opening using dynamic contrast-enhanced MRI. Phys Med Biol. 2010; 55:5451–5466. [PubMed: 20736501]

[181]. Raymond SB, Hynynen K. Acoustic transmission losses and field alterations due to human scalp hair. IEEE Trans. Ultrason. Ferroelectr. Freq. Contr. 2005; 52:1415–1419.

[182]. Park J, Zhang Y, Vykhodtseva N, Akula JD, McDannold NJ. Targeted and Reversible Blood-Retinal Barrier Disruption via Focused Ultrasound and Microbubbles. PLoS One. 2012; 7:e42754. [PubMed: 22912733]

[183]. Wachsmuth, J.; Chopra, R.; Hynynen, K. Feasibility of Transient Image-guided Blood-Spinal Cord Barrier Disruption. Proceedings of the 8th International Symposium on Therapeutic Ultrasound; Minneapolis, MN: AIP Conf.Proc; 2008. p. 256-259.

[184]. Fischer K, McDannold NJ, Zhang Y, Kardos M, Szabo A, Szabo A, Reusz GS, Jolesz FA. Renal ultrafiltration changes induced by focused US. Radiology. 2009; 253:697–705. [PubMed: 19703861]

[185]. McDannold NJ, Vykhodtseva NI, Hynynen K. Microbubble contrast agent with focused ultrasound to create brain lesions at low power levels: MR imaging and histologic study in rabbits. Radiology. 2006; 241:95–106. [PubMed: 16990673]

[186]. Borrelli MJ, O'Brien WD Jr. Hamilton E, Oelze ML, Wu J, Bernock LJ, Tung S, Rokadia H, Culp WC. Influences of microbubble diameter and ultrasonic parameters on in vitro sonothrombolysis efficacy. J Vasc. Interv Radiol. 2012; 23:1677–1684. [PubMed: 23106936]

[187]. Czarnota GJ, Karshafian R, Burns PN, Wong S, Al Mahrouki A, Lee JW, Caissie A, Tran W, Kim C, Furukawa M, Wong E, Giles A. Tumor radiation response enhancement by acoustical stimulation of the vasculature. Proc Natl. Acad. Sci. U. S. A. 2012; 109:E2033–E2041. [PubMed: 22778441]

[188]. Yang FY, Fu WM, Chen WS, Yeh WL, Lin WL. Quantitative evaluation of the use of microbubbles with transcranial focused ultrasound on blood-brain-barrier disruption. Ultrason. Sonochem. 2008; 15:636–643. [PubMed: 17910929]

[189]. McDannold N, Vykhodtseva N, Hynynen K. Use of ultrasound pulses combined with Definity for targeted blood-brain barrier disruption: A feasibility study. Ultrasound Med. Biol. 2007; 33:584–590. [PubMed: 17337109]

[190]. Lin KJ, Liu HL, Hsu PH, Chung YH, Huang WC, Chen JC, Wey SP, Yen TC, Hsiao IT. Quantitative micro-SPECT/CT for detecting focused ultrasound-induced blood-brain barrier opening in the rat. Nucl. Med Biol. 2009; 36:853–861. [PubMed: 19720297]

[191]. Yang FY, Wang HE, Lin GL, Lin HH, Wong TT. Evaluation of the increase in permeability of the blood-brain barrier during tumor progression after pulsed focused ultrasound. Int. J Nanomedicine. 2012; 7:723–730. [PubMed: 22359451]

[192]. Huang Q, Deng J, Xie Z, Wang F, Chen S, Lei B, Liao P, Huang N, Wang Z, Wang Z, Cheng Y. Effective gene transfer into central nervous system following ultrasound microbubbles-induced opening of the blood-brain barrier. Ultrasound Med. Biol. 2012; 38:1234–1243. [PubMed: 22677255]

[193]. Etame AB, Diaz RJ, O'Reilly MA, Smith CA, Mainprize TG, Hynynen K, Rutka JT. Enhanced delivery of gold nanoparticles with therapeutic potential into the brain using MRI-guided focused ultrasound. Nanomedicine. 2012

[194]. Wang PH, Liu HL, Hsu PH, Lin CY, Wang CR, Chen PY, Wei KC, Yen TC, Li ML. Gold-nanorod contrast-enhanced photoacoustic micro-imaging of focused-ultrasound induced blood-brain-barrier opening in a rat model. J Biomed. Opt. 2012; 17:061222. [PubMed: 22734752]

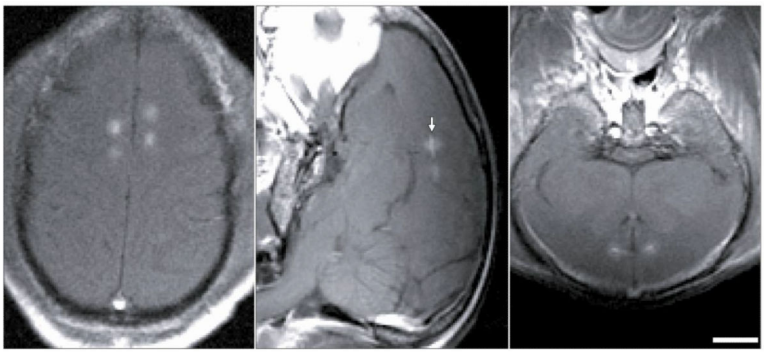

Figure 1.

Contrast-enhanced T1-weighted MRI of the brain of a rhesus macaque showing enhancement at four focal targets in the cingulate cortex after injection of Gd-DTPA. (Left image: Axial; Middle: Sagittal; Right: Coronal). Enhancement of this MRI contrast agent, which normally does not extravasate into the brain, indicates areas with BBB disruption. Four targets were sonicated using a 220 kHz clinical MRI-guided FUS system along with an infusion of Definity microbubbles. The dimensions of the disrupted spots were approximately 3 mm wide and 4 mm long. Note the leakage of contrast agent into the cingulate sulcus evident in the sagittal image (arrow). These images were obtained in a study evaluating passive cavitation mapping during microbubble-enhanced FUS [176] (bar: 1 cm)

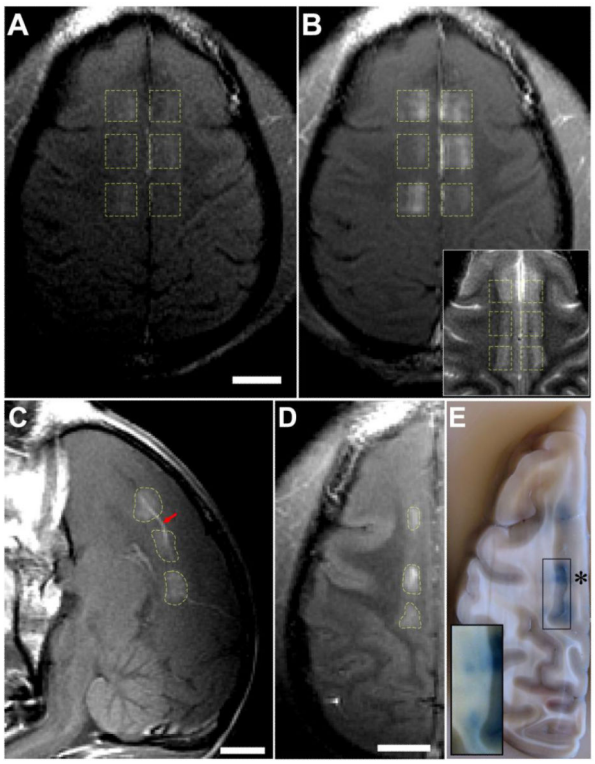

Figure 2.

Demonstration of FUS-induced BBB disruption using contrast enhanced MRI and trypan blue. (**A–C**) Contrast-enhanced T1-weighted MRI after BBB disruption at six volumes in the cingulate cortex. At each volume, the focal region was steered electronically in sequence to nine targets in a 3×3 grid using a phased array. **(A)** Low-level enhancement observed with gadofosveset trisodium, an MR contrast agent that binds to albumin in the blood (MW of albumin: ~67 kDa); it was administered before sonication. **(B)** Enhancement after injection of Gd-DTPA (MW: 938 Da). The inset in **(B)** shows the same view in T2-weighted imaging. The enhancement patterns correspond to regions of cortical gray matter visible in T2-weighted imaging. **(C)** Sagittal view of Gd-DTPA enhancement, which included leakage of agent into a sulcus (arrow). **(D–E)** Volumetric BBB disruption at three targets centered on the boundary between the cingulate cortex and white matter; from another experimental session in this animal. **(D)** T1-weighted MRI showing Gd-DTPA extravasation in the cingulate cortex, but not in the white matter. **(E)** Photograph of formalin-fixed brain showing trypan blue extravasation into both the cingulate cortex and white matter. This differential enhancement between gray and white matter presumably reflects differences in vascular density. The white matter component of two of these targets is shown with increased image contrast in the inset to better visualize low-level trypan blue extravasation. (scale bars: 1 cm). Reprinted from Cancer Research 2012; 72:3652–3663; © 2012 American Association for Cancer Research

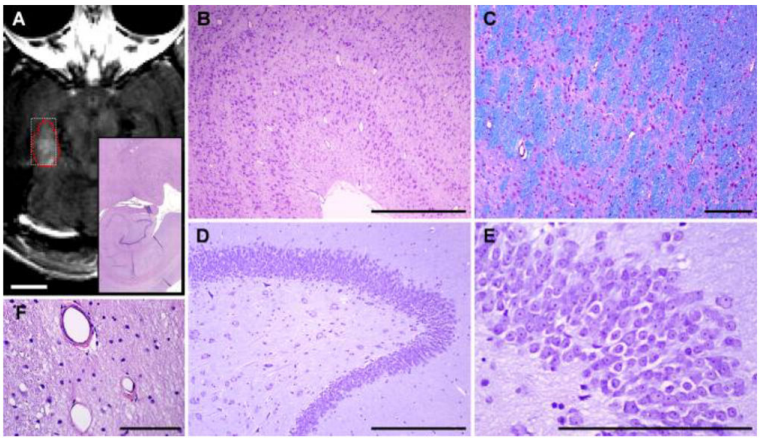

Figure 3.

Normal-appearing histology after FUS-induced BBB disruption. This example was obtained after volumetric sonication to induce BBB disruption in the hippocampus and lateral geniculate nucleus (LGN) in macaque. This target was sonicated approximately two hours before the animal was sacrificed and in seven prior sessions over several months. **(A)** Axial contrast-enhanced T1-weighted MRI showing BBB disruption induced by sonicating nine targets in a 3×3 grid. **(B)** Low-magnification microphotograph showing histology in the hippocampus/LGN. **(C–D)** High-magnification views showing normal-appearing layers in the LGN. **(E–G)**: High-magnification views of hippocampus showing the granular cell layer **(E)** and the pyramid layers **(F–G)**. H: Blood vessels in the LGN with a few extravasated red blood cells, presumably from the last sonication session. Only a very small number of such extravasations were found. (**B–G**: Nissl; H: H&E; scale bars: **A**: 1 cm, **B**–**D**: 1 mm, **E–H**: 200 μm). Reprinted from Cancer Research 2012; 72:3652–3663; © 2012 American Association for Cancer Research.

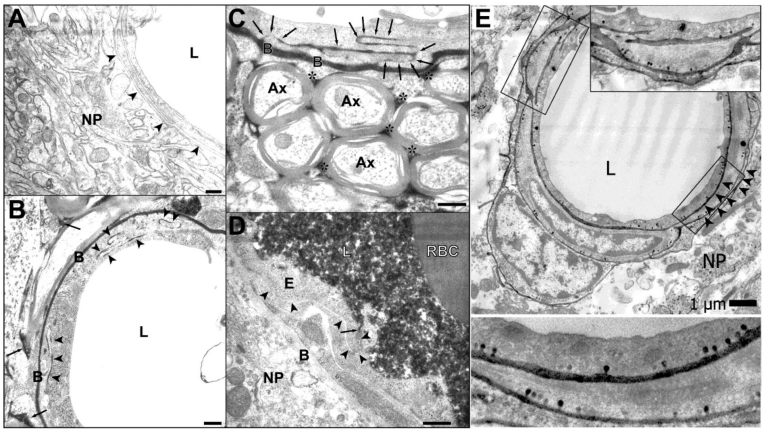

Figure 4.

BBB permeability for horseradish peroxidase (HRP). **(A)** Photomicrograph showing part of a cross-sectioned microvessel and the surrounding nerve tissue from a nonsonicated area. No HRP passage to the basement membrane (arrowheads) or the neuropil (NP) can be seen. The lumen (L) appears empty because the tracer was washed out during perfusion fixation. **(B)** A portion of a microvessel with adjacent nerve tissue from a sample obtained 1 h after sonication. Passage of HRP (black color) through several interendothelial clefts is indicated by arrowheads. The tracer has infiltrated the basement membrane (B) and the interstitial space (arrows) in the neuropil. **(C)** A portion of longitudinally sectioned capillary in a sample obtained 2 h after sonication. The tracer is present in the junctional cleft (arrows), the basement membrane (B) and the interstitial spaces (asterisks) between myelinated axons (Ax). **(D)** Full restoration of the tight junctional barrier function 4 h after sonication. Immersion fixation (instead of perfusion fixation) was used in this brain and permits visualization of the tracer (black) filling the lumen (L) and being stopped at the first tight-junction (arrow). No penetration can be seen in the rest of the junctional cleft (arrowheads), nor in the basement membrane (B) or neuropil (NP). E: endothelial cell cytoplasm; RBC: red blood cell in the lumen. Scale bars: 200 nm. Modified from Ultrasound in Med. & Biol., Vol. 34, No. 7, pp. 1093–1104, 2008; Copyright © 2008 World Federation for Ultrasound in Medicine & Biology. **(E)** Electron micrograph of an arteriole 1 h after sonication at 0.26 MHz. An intense vesicular transport is demonstrated by the increased number of HRP-positive caveolae (arrows). Significantly fewer vesicles were observed in capillaries and venules. L: lumen. Modified from Ultrasound in Med. & Biol., Vol. 32, No. 9, pp. 1399–1409, 2006; Copyright © 2006 World Federation for Ultrasound in Medicine & Biology

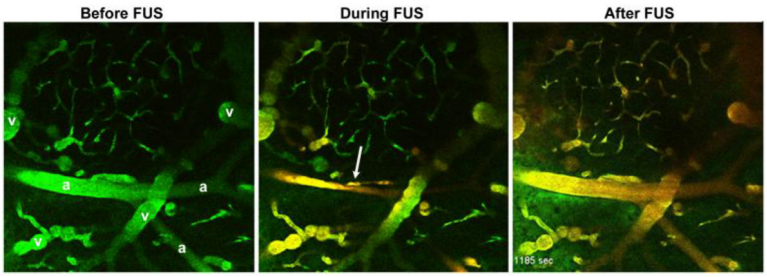

Figure 5.

Vascular effects observed in real time during FUS-induced BBB disruption using in vivo multiphoton microscopy. Each frame is a 615×615 μm image acquired using in a mouse before, during, and approximately 20 min after sonication. Arterioles and veins (determined by dye transit) are marked `a' and `v' respectively, in the first frame. The animal received 0.1mL (2 mg/mL) 10 kDa, dextran-conjugated Alexa Fluor 488 intravenously ~5 mins before imaging (green in images) Immediately after the first frame was taken, a 45-sec US exposure was initiated and a 0.1mL bolus (10 mg/mL) of 70 kDa, dextran-conjugated Texas Red was delivered intravenously (red in images). Almost total occlusion of the large vessel in the center of the field occurred 12 secs after the initiation of US (arrow). Beginning at 60 secs and by 305 secs, leakage in the green channel is apparent in the lower left of the field, and around the central vessel. Modified from Journal of Cerebral Blood Flow & Metabolism 2007;27(2):393–403; Copyright © 2006 ISCBFM.

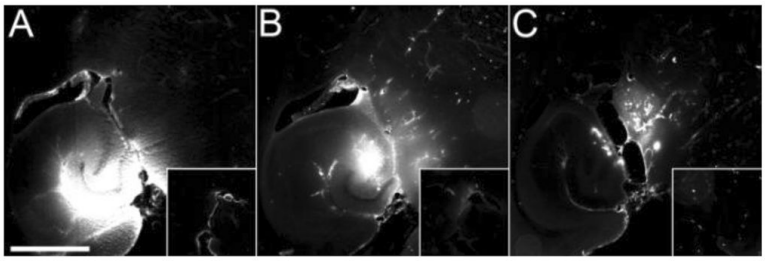

Figure 6.

Delivery of fluorescent dextrans with different sizes across the BBB in a mouse using FUS and microbubbles (A: 3 kDa; B: 10 kDa; C: 70 kDa; bar: 1 mm). Diffuse fluorescence regions can be observed for all dextrans, whereas spots of high fluorescence are observed only with the 70-kDa dextran. Modified from Proc Natl Acad Sci U S A 2011; 108: 16539–16544; © 2011 by The National Academy of Sciences of the USA.

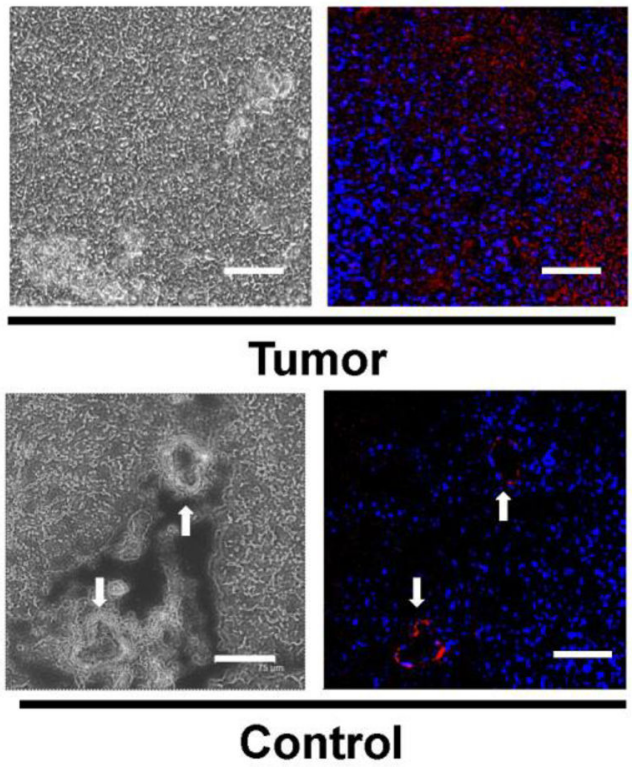

Figure 7.

Confocal micrographs of tissue from tumor after FUS-induced BTB permeabilization followed by magnetic targeting and contralateral brain regions after delivery of magnetic nanoparticles (MNPs) loaded with epirubicin. Dark structures in the phase micrographs show MNPs (Left); fused fluorescence images (Right) indicate the presence of epirubicin (red) and DAPI-stained nuclei (blue). Arrows indicate the capillaries; epirubicin occurs in the capillary beds but does not penetrate into the brain parenchyma. Modified from Proc Natl Acad Sci U S A 2010; 107: 15205-15210; © 2011 by The National Academy of Sciences of the USA.

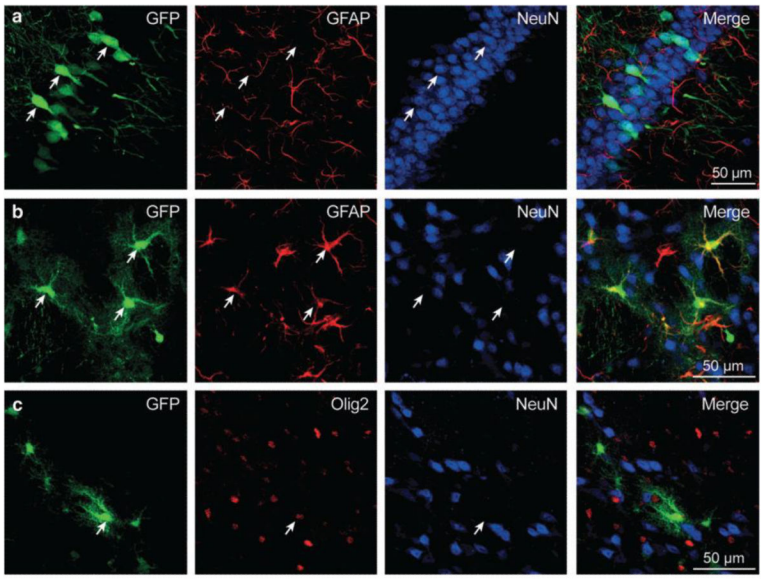

Figure 8.

Gene transfer to neurons, astrocytes, and oligodendrocytes after delivery of adeno-associated virus serotype 9 carrying the green fluorescent protein (GFP) to the mouse brain via FUS-induced BBB disruption. Immunohistochemistry was used to detect GFP expression in hippocampus for (a) NeuN-positive cells (neurons, white arrows), and striatum for (b) GFAP-positive cells (astrocytes, white arrows) and (c) Olig2-positive cells (oligodendrocytes, white arrow). Modified from Human Gene Therapy 23:1144–1155 (November 2012); © 2012 Mary Ann Liebert, Inc.

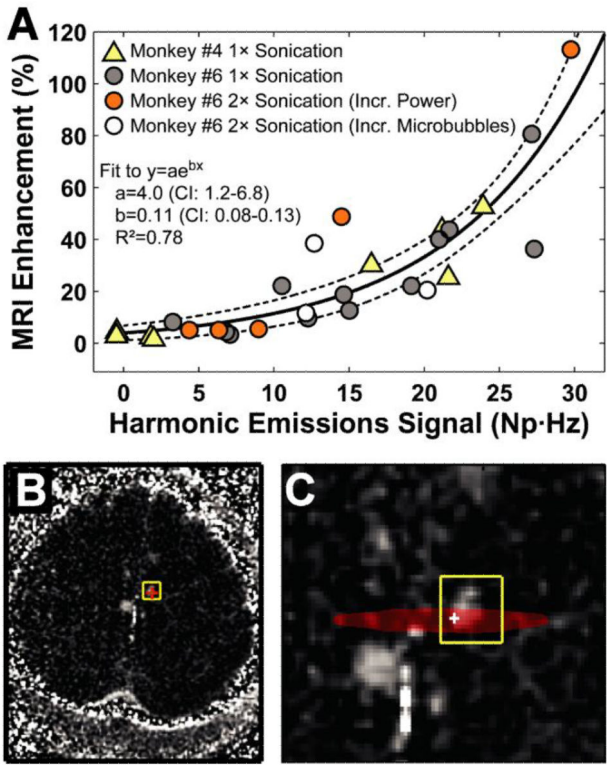

Figure 9.

Comparison of MRI signal enhancement with microbubble acoustic emissions. **(A)** MRI signal enhancement after Gd-DTPA injection plotted as a function of the harmonic emissions signal strength measured with single-element detectors. A clear relationship between the two measurements was observed with a good fit to an exponential. The agreement appeared to hold among different animals and in cases where targets with low-level harmonic emissions were sonicated a second time with either a higher power level or an increased dose of microbubbles. Reprinted from PLoS ONE 7(9): e45783. doi:10.1371/journal.pone.0045783; © 2012 Arvanitis et al. **(B–C)** Comparison between MRI signal enhancement and passive cavitation mapping. **(B)** Map showing the enhancement relative to a pre-contrast image. **(C)** Fusion of passive acoustic map with the T1-weighted MRI from **(B)**. The red region shows the pixels in the cavitation map within 95% of the maximum value. This region overlapped with the contrast enhancement. The pixel with the maximum cavitation activity is noted with a “+”. The enhancement from other targets sonicated in the same session is visible; Modified from Phys Med Biol 58.14 (2013): 4749–61; © 2013 Institute of Physics and Engineering in Medicine.

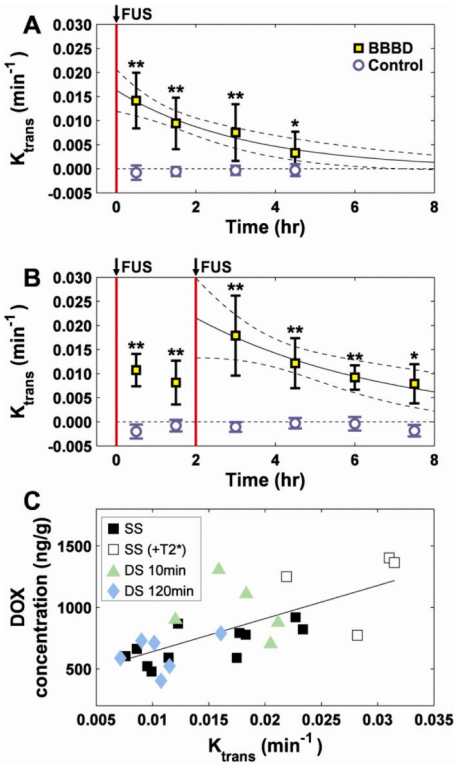

Figure 10.

Using DCE-MRI to evaluate FUS-BBB disruption. **(A–B)** Mean K_{trans} values measured vs. time from DCE-MRI in regions of interest at sonicated locations and in corresponding non-sonicated structures in the contralateral hemisphere. The decay of K, which occurred due to restoration of the BBB, was fit to an exponential decay (solid line; dotted lines: 95% CI). **(A)** Decay after a single sonication. **(B)** Time course after two sonications separated by 120 min. The second sonication increased the amount of time the barrier was disrupted. Values were significantly higher than in control locations in the contralateral hemisphere (**P<0.01 and *P<0.05). **(C)** DOX concentration achieved at the sonicated locations as function of K_{trans} measured using DCE-MRI 30 min after sonication. The DOX concentration was measured approximately 16 hrs later for brain targets in single sonication (SS), single sonication with hyperintense spots in T2* weighted image (SS (+ T2*)), double sonication with 10 min interval (DS 10 min), and double sonication with 120 min interval (DS 120 min). The solid line shows a linear regression of the data (slope: 28,824 ng/g DOX per change in K_{trans} in min^{-1}; intercept: 377 ng/g DOX; R: 0.7). Modified from Journal of Controlled Release 2012;162:134–142; © 2012 Elsevier B.V.

Table 1

Different methods investigated to get around the BBB to deliver drugs to the brain

Method	Advantages	Disadvantages
Direct injection, convection-enhanced delivery, implantable devices	High local drug concentrations can be achieved; systemic administration avoided.	Invasive; side effects; challenging to control; not readily repeatable.
Intrathecal, intraventricular injection	Effectively delivers drugs to subarachnoid space, brain surface.	Little drug penetration beyond brain surface; invasive.
Trans-nasal delivery	Noninvasive; easy to administer; repeatable.	Small volume of drug delivered; interindividual variability.
BBB disruption via arterial injection of osmotic solution or other agents	Effectively delivers drugs to large brain regions; large clinical experience.	Invasive; requires general anesthesia; side effects; not readily repeatable.
Modification of drugs to cross barrier through endogenous transport mechanisms	Easily administered; delivered to whole brain.	Requires systemic administration; expensive; each drug requires new development; clinical data lacking.
BBB disruption via FUS and microbubbles	Noninvasive; readily repeatable; can target drug delivery to desired volumes; can control “magnitude” of disruption; can be combined with drug-loaded microbubbles or magnetic particles for additional targeting.	Requires systemic administration; currently technically challenging; large volume/whole brain disruption unproven; no clinical data.

Table 2

Reported effects of different parameters on BBB disruption via FUS and microbubbles

Parameter	Effect on BBB disruption
Pressure amplitude	Increase in BBB disruption magnitude as pressure amplitude increases; saturation at some point [82–84]; vascular damage produced at high pressure amplitudes.
Ultrasound frequency	Decrease in BBB disruption threshold as frequency decreases; some evidence of improved safety for lower frequencies [85].
Burst length	For burst lengths less than 10 ms, BBB disruption threshold increases and BBB disruption magnitude decreases as burst length is reduced [86,90–92]; little or no increase in disruption magnitude for longer bursts [77,81,90].
Pulse repetition frequency	BBB disruption magnitude increases as repetition frequency increases up to a point [90]. Other works have observed no effect on BBB disruption magnitude [86].
Ultrasound contrast agent dose	Magnitude of BBB disruption increases with dose [83,90,94,188]; other experiments have reported no effect [86].
Sonication duration	Longer durations [84] or repeated sonication [96,97] increase magnitude of BBB disruption; damage reported with excessive sonication [84,97].
Microbubble diameter	Threshold for BBB disruption lower for larger microbubbles; disruption magnitude increased with larger microbubbles [87–89].
Ultrasound contrast agent	Similar outcomes reported for Optison® and Defmity® microbubbles [189]. Sonovue® microbubbles and research agents are also commonly used.

Table 3

Example different tracers that have been delivered across the BBB

Agent	Size	Use
Lanthanum chloride	139 Da	Electron microscopy tracer [109]
99mTc-Diethylenetriaminepentaacetic pentaacetate	492 Da	SPECT agent [190]
Omniscan® (Gd-DTPA-BMA)	574 Da	MRI contrast agent [89]
Magnevist® (Gd-DTPA)	928 Da	MRI contrast agent [77]
Trypan blue, Evans blue	~67 kDa	Tissue dyes (binds to albumin) [79,191]
Ablavar® (Gadofosveset trisodium)	~67 kDa	MRI contrast agent (binds to albumin) [79]
Horseradish peroxidase	40 kDa	Electron microscopy tracer [78]
Dextran	3–70 kDa	Fluorescent tracer [136]
Immunoglobulin G	~150 kDa	Endogenous antibodies [157]
pCMV-EGFP[1]	?	PlasmidDNA [192]
MION-47	20 nm	MRI contrast agent [120]
Gold nanoparticles	50 nm	Carrier for drugs or imaging [193]
Gold nanorods	10×40 nm	Photoacoustic imaging contrast agent [194]
Dotarem, P846, P792, P904, P03680	1–65 nm	MRI contrast agents [115]

[1] Loaded into a microbubble

Table 4

Example therapeutic agents that have been delivered across the BBB or BTB

Therapeutic Agent	Size	Use	Delivered to
Temozolomide	194 Da	Chemotherapy	Glioma model (9L)[1] [141]
1,3-bis(2-choroethyl-1-nitrosourea (BCNU)[2]	214 Da	Chemotherapy	Glioma model (C6)[1] [138,152]
Cytarabine	243 Da	Chemotherapy	Normal brain [140]
Boronophenylalanine	330 Da	Agent for boron neutron capture therapy	Glioma models (GBM 8401 [149]; 9L [150])
Doxorubicin	540 Da	Chemotherapy	Normal brain [96]
Methotrexate	545 Da	Chemotherapy	Normal brain [139]
siRNA	~13 kDa	Huntington's disease therapy	Normal brain [135]
Glial cell line-derived neurotropic factor (GDNF)[2]	24kDa	Neuroprotective agent	Normal brain [153]
Brain-derived neurotropic factor (BDNF)	27 kDa	Neuroprotective agent	Normal brain[3] [156]
Herceptin (Trastuzumab)	148 kDa	Anti-cancer antibody	Normal brain [147]; Breast cancer brain met. model (BT474)[1] [148]
BAM-10 Aβ targeted antibodies	~150 kDa	Therapeutic antibody for Alzheimer's Disease	TgCcrND8 Alzheimer's model mice[1] [158]
BCNU-VEGF[2]	~150 kDa	Antiangiogenic-targeted chemotherapy	Glioma model (C6)[1] [155]
Plasmid DNA (pBDNF-EGFP)[2]	~3600 kDa[4]	Gene therapy	Normal brain [154]
Epirubicin in Magnetic nanoparticles	~12 nm	Magnetic targeted chemotherapy	Glioma model (C6)[1] [144]
Doxorubicin in magnetic nanoparticles[2]	~6–10 nm	Magnetic targeted chemotherapy	Glioma model (C6) [146]
BCNU in magnetic nanoparticles	~10–20 nm	Magnetic targeted chemotherapy	Glioma model (C6)[1] [145]
Adeno-associated Virus (AAV)	~25 nm	Gene therapy vector	Normal brain [160–162]
Liposomal doxorubicin (Lipo-DOX)	90 nm	Chemotherapy	Normal brain [83]; Glioma model (9L)[1] [142,163]
Interleukin-4 receptor targeted Lipo-DOX	100–120 nn	l Chemotherapy	Glioma model (8401) [143]
Neural progenitor cells	7–10 μm	Stem cell	Normal brain [159]
Natural killer cells (NK-92)	~10 μm	Cell therapy for brain tumor	Breast cancer brain met. model (MDA-MB-231-HER2) [151]

[1] Also showed improved outcomes with FUS-induced BBB disruption

[2] Used drug-loaded microbubbles

[3] Also showed drug activity after delivery

[4] Assumed 660 Da per base pair (bp), 760 bp for BDNF, and 4700 bp for pEGFP-N1